

Article

The Influence of Distributed Generation on the Operation of the Power System, Based on the Example of PV Micro-Installations

Norbert Chamier-Gliszczyński ^{1,*}, Grzegorz Trzmiel ², Jarosław Jajczyk ², Aleksandra Juszcak ²,
Waldemar Woźniak ³, Mariusz Wasiak ^{4,*}, Robert Wojtachnik ⁵ and Krzysztof Santarek ⁵

¹ Faculty of Economics, Koszalin University of Technology, 75-453 Koszalin, Poland

² Faculty of Control, Robotics and Electrical Engineering, Poznan University of Technology, 60-965 Poznan, Poland

³ Faculty of Mechanical Engineering, University of Zielona Gora, 65-001 Zielona Gora, Poland

⁴ Faculty of Transport, Warsaw University of Technology, 00-662 Warsaw, Poland

⁵ Faculty of Mechanical and Industrial Engineering, Warsaw University of Technology, 02-524 Warsaw, Poland

* Correspondence: norbert.chamier-gliszczyński@tu.koszalin.pl (N.C.-G.); mariusz.wasiak@pw.edu.pl (M.W.)

Abstract: This article describes the problems associated with distributed electrical power generation and the most frequent interruptions occurring in power grids. The most common methods of improving the quality of the power supply were analyzed and the possibilities offered by energy storages in this respect were considered. The operating parameters of an exemplary PV system connected to the power grid were analyzed. For this purpose, the model implemented in the Matlab/Simulink environment was used. Based on the conducted analysis and a review of the literature, conclusions were drawn and solutions were presented which could improve the quality and the reliability of power supply. The simulations conducted focused on the co-operation of individual photovoltaic, micro-installations, with rated powers of 12.2, 19.825, and 39.65 Kw in the power grid, which also corresponds to the co-operation of several, smaller micro-installations with low density.



Citation: Chamier-Gliszczyński, N.; Trzmiel, G.; Jajczyk, J.; Juszcak, A.; Woźniak, W.; Wasiak, M.; Wojtachnik, R.; Santarek, K. The Influence of Distributed Generation on the Operation of the Power System, Based on the Example of PV Micro-Installations. *Energies* **2023**, *16*, 1267. <https://doi.org/10.3390/en16031267>

Academic Editors: Abdelali El Aroudi and Alon Kuperman

Received: 21 November 2022

Revised: 17 January 2023

Accepted: 20 January 2023

Published: 25 January 2023



Copyright: © 2023 by the authors. Licensee MDPI, Basel, Switzerland. This article is an open access article distributed under the terms and conditions of the Creative Commons Attribution (CC BY) license (<https://creativecommons.org/licenses/by/4.0/>).

Keywords: distributed generation; photovoltaic micro-installation; power system; power supply quality; modelling

1. Introduction

In recent years, the share of distributed electrical power generation in the overall power system has grown. The dynamic development of renewable energy sources, primarily including photovoltaic power systems is a fact. The energy independence of households and enterprises is an appropriate response to the threats appearing on the energy market and to the continuous, very dynamic increase in energy prices. This applies to all sectors of the economy, including, in particular, transport [1] and railway transport [2,3], where efforts are being intensified to replace internal combustion engines with electric ones [4,5].

Electric energy consumption by road vehicles at the level of 0.14–0.24 kWh/km (depending on the load) [6], in view of the multiple electricity price increases (approximately 6–7 fold compared to 2019), makes electric drives economically much less competitive than classic drives, even though fuel prices have nearly been doubled (similar significant changes in terms of the competitiveness of low-emission drives also took place in the case of vehicles powered by LNG gas [7]). Currently, taking into account the wholesale prices of fuels and electricity prices for enterprises, the cost of energy consumption by an EV per kilometer is similar to the cost of fuel consumption by a vehicle with a classic drive. Therefore, the most promising direction for the development of electromobility [8,9] in the face of a number of threats influencing the instability of the energy market, also in the economic dimension, seems to be only a combination of investing in electric vehicles [10] and infrastructure for charging these vehicles with investing in their own renewable energy

sources, in particular in photovoltaics [11]. There are innovative solutions in the civil engineering industry that enable integration of photovoltaic systems with various architectural elements (e.g., with the facade of buildings) [12,13].

Nowadays a large number of distributed energy sources and their expected further rapid growth means that the problem of their impact on power grids must be investigated. Efforts should be made to develop tools enabling computational research in this area, taking into account, also, the various strategies limiting this impact.

Traditional, centralized distribution networks are so called reactive networks. This means that the energy flows in a constant direction, i.e., from the transformer-switching station, which is the power center, to individual consumer centers. Currently, when the connection of a greater and greater number of distributed energy sources to the network is observed, the distribution networks are becoming active networks, in which the energy flow occurs in two directions at the same time. All sources connected to the network introduce active power to it and its value may differ from the local demand at a given time. This affects the quality of energy, the reliability of its supply as well as security of the power system. The concept of the energy quality usually refers to the quality of supply voltage. It should have a constant frequency and rms value; the voltage vectors of each of the three phases should form a symmetrical system with a compliant sequence, and the waveform of voltage should be sinusoidal. Various electromagnetic interruptions occur, both under normal operating conditions of the system and at the time of interferences. Among the most frequent interruptions in power systems, it is necessary to distinguish, above all, changes in the rms and supply voltage frequency, voltage asymmetry and voltage dips as well as occurrence of higher current and voltage harmonics [14,15]. They have all been described, in detail, in Section 1.2.

Connecting PV micro-installations to the grid generates a number of problems that have to be resolved by power system operators. The solution to the problem may involve the creation of the simulation of operation of the system in the Matlab/Simulink environment [16]. This article focusses on the impact of individual PV micro-installations on the operation of the power system, which is most often encountered in practice, on a daily basis. The program allows different states of the system to be simulated, namely, checking how high the level of interruptions occurring is and whether it is necessary to apply power improvement measures. Sections 1.1–1.5 describe the most frequently occurring interruptions and their causes.

1.1. Changes in the Root Mean Square and Supply Voltage Frequency

A change in voltage is a change in the mean square root of the voltage in the same given point of the grid in consecutive moments. The most frequent cause of the change in voltage in power system nodes are the continuously occurring load changes. These cause voltage drops on the respective elements of the power grid. Other factors which may cause changes in voltage are as follows [14,16]:

Switching operations on power grids aimed at changing the topology of the grid or eliminating contingencies;

Control processes in power plants, whose aim is to balance the generation and consumption of electricity;

Changes in load resulting from switching loads on and off and the operation of loads with variable power consumption.

The supply voltage frequency is among the most important indicators of the quality of electricity. Its rated value is equal to 50 Hz and is the same at each point of the Polish power system. The value of the frequency depends on the balance of active power generated in energy sources and used in loads. It is assumed that the normal operating state of the system is when the voltage frequency ranges between 49.85 and 50.15 Hz. Its maintenance within such limits requires the maintenance of reserves of available active power in the power system, with the help of which it will be possible to balance load variations and power losses occurring in transmission and distribution networks. When the frequency

falls below 49.2 Hz or rises above 51.5 Hz an emergency state occurs. In such a case, the system's defense plans may be implemented. However, if the frequency falls below 47.5 Hz or rises above 52.5 Hz, there is a systemic failure. In this situation, the only solution is to implement the system reconstruction plans. In order to maintain the root mean square voltage at the set level, appropriate control methods must be applied [17].

1.2. Voltage Fluctuations

Voltage fluctuations are rapid changes in the rms of the voltage occurring during steady state operation of power grids. Their occurrence may be caused by connecting the so-called disturbing loads, which draw power in a rapidly changing and difficult to predict manner. Voltage fluctuations may also be the result of certain types of sources. Wind farms have the greatest impact on the power system, as they often have generators with large capacities installed, and changes in generation of this power is significant. This is because the active power generated depends on the wind direction and its speed, squared. The graphs in Figures 1 and 2 show the changes in the rms voltage: at the terminals of a wind turbine in Figure 1 and the hydroelectric power plant at the grid connection point in Figure 2. When comparing the two graphs, it can be concluded that the wind turbine is characterized more by higher amplitudes and the frequency of voltage changes than by the hydroelectric generating set [18].

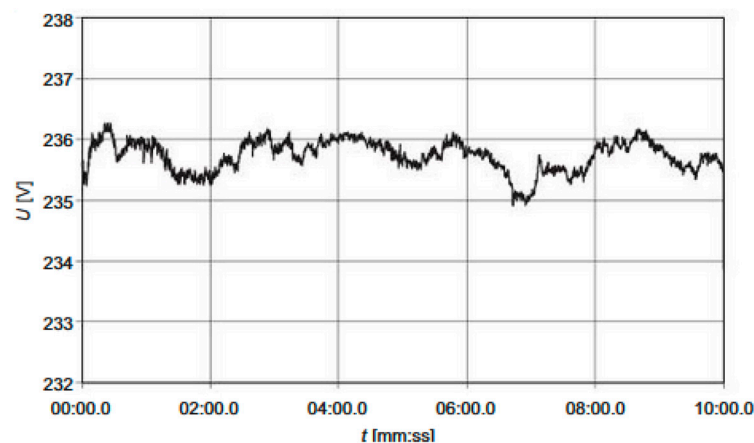


Figure 1. Changes in rms value voltage at the terminals of the wind turbine [18].

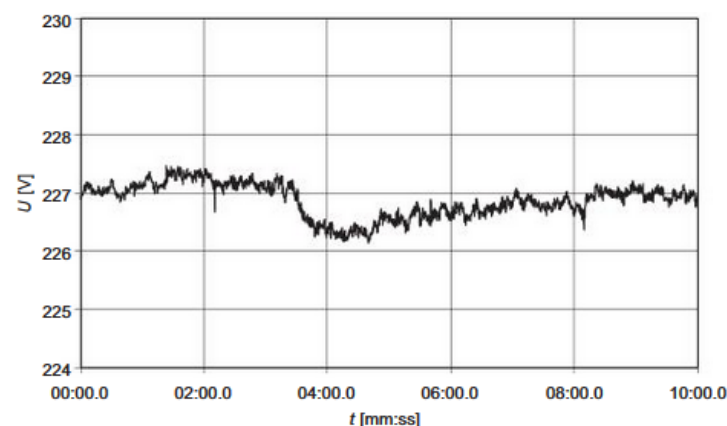


Figure 2. Changes in rms voltage at the terminals of the hydroelectric power plant generator [18].

Voltage fluctuations bring many negative effects for the operation of the power system and the loads connected to it. They may affect the torque of electrical machinery and consequently, the slip value and the whole process. They also lead to a reduction in the service life of machinery by accelerating the wear of rotors and causing increased mechanical vibrations.

Among the effects of voltage fluctuations or, to be more precise, the transfer of these fluctuations to the low voltage network, most noticeable for the recipient, is the phenomenon of light flickering. “This is a subjective sense of change in light flux, whose luminance or spectral distribution is subject to changes over time” [18]. The flickering of light has a very negative effect on man’s well-being as well as on quality and work conditions.

The effects of voltage fluctuations are affected mostly by their amplitude and frequency of occurrence. The frequency of appearance of voltage fluctuations is determined, above all, by the type of load and the nature of its operation. The amplitude of voltage fluctuations depends on the power supply system of disturbing loads. It can be reduced in two ways. The first one is to reduce changes in reactive power in the mains by using capacitors and dynamic stabilizers. They cause the flow of reactive current of the fundamental harmonic, which results in the reduction in voltage on power supply network impedances. Another method of reducing voltage fluctuations is the increase in the short-circuit power at the point of connection of the disturbing load while keeping the power of the load constant (Figure 3). The short-circuit power allows the grid stiffness in a given node to be assessed. The higher the assumed value of the short-circuit power, the higher the grid stiffness; therefore, the amplitude of voltage fluctuations is then relatively small [18–21].

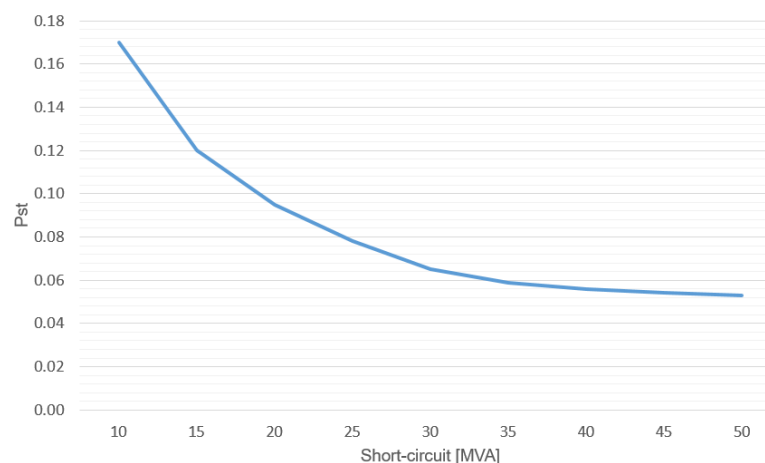


Figure 3. Dependence of the voltage fluctuation factor on the short-circuit power at the point of connection.

An increase in the short-circuit power can be achieved using several methods, i.e., by [22,23]:

- Connection of the load to buses with higher rated voltage,
- Separation of the disturbing load or group of disturbing loads by separating the lines directly from the high voltage network intended for supplying the given group of loads or supplying the quiet and disturbing loads from separate windings of three-winding transformers or from separate transformers,
- Increasing the power of a transformer supplying a series load, and
- Installing series capacitors.

1.3. Voltage Asymmetry

The voltage at the loads is symmetrical, if the components of the power system are linear and symmetrical and the load on the different phases is the same. This means that the voltages at the terminals of the synchronous generators have the same rms values and the vectors of these voltages are offset from each other by 120 electrical degrees. In practice, it is rarely possible to obtain complete symmetry in all points of the system, as many loads connected to the low-voltage and high-voltage networks are asymmetrical. In consequence, the flow of phase currents with different values and the occurrence of asymmetrical voltage losses are observed in the network. The differences in the values of the self-impedances and mutual impedances of the transmission system’s components in individual phases may also be the cause of the asymmetry. The factors which often

contribute to the voltage asymmetry in the system, usually short lasting, are asymmetrical short-circuits. The limitation of the frequency and duration of short-circuits by, among other things, the selection of appropriate protection settings is of key significance [24]. Analysis and modelling of the asymmetrical operating states of the power system are both complicated tasks. For this reason, the method of symmetrical components is often used to analyze the asymmetrical operating states. In such a case, the asymmetrical 3-phase system is replaced by three symmetrical 3-phase systems—direct, inverse and zero. Phenomena taking place in each of the three systems are subject to analysis, and then they are referred to the asymmetrical system [20,21].

In order to determine the level of asymmetry, the asymmetry coefficient K is used. It is the ratio of the inverse component and/or zero component to the direct component of voltage [18]:

$$K_{2U} = \frac{U_{2(1)}}{U_{1(1)}} \cdot 100\% \quad K_{0U} = \frac{U_{0(1)}}{U_{1(1)}} \cdot 100\% \quad (1)$$

where $U_{2(1)}$ —rms of the inverse component of voltage, $U_{1(1)}$ —rms of the direct component of voltage, and $U_{0(1)}$ —rms of the zero component of voltage.

Index 1 provides information that the values refer to the first supply voltage harmonic.

1.4. Voltage and Current Harmonics

Higher voltage and current harmonics are components of voltage or current with frequencies that are integral multiples of the fundamental frequency equal to 50 Hz. The source of higher harmonics are loads with non-linear voltage–current characteristic. As a result of the uptake of higher harmonics by these loads, distorted voltage drops are observed on the grid elements and, consequently, distortion of the sinusoidal waveforms of the supply voltages. The time waveforms of distorted currents and voltages can be described mathematically by the Fourier series [18]. The degree of voltage distortion depends both on the value of harmonics introduced into the grid and on the grid stiffness. The higher the power grid impedance and thus the lower the short-circuit power in the point of common coupling, the higher the voltage distortion will be. This means that the propagation of harmonic currents introduced by the source is mainly towards the low-voltage grid. The rms voltage of the higher harmonic of voltage in the i -th node of the grid is calculated using the following formula [18]:

$$U_{ih} = Z_{i ih} \cdot I_{ih} + \sum_{\substack{j=1 \\ j \neq i}}^N Z_{i j h} \cdot I_{jh} \quad (2)$$

where $Z_{i ih}$ —self-impedance of the node for the h -th harmonic, $Z_{i j h}$ —mutual impedance of nodes i, j for the h -th harmonic, I_{ih} —source current of the h -th harmonic in node i , I_{jh} —source current of the h -th harmonic in node j , and N —number of network nodes.

In order to determine the degree of distortion of the voltage signal by higher harmonics, the relative values of higher voltage harmonics are referred to the rms of the fundamental harmonic [18]:

$$U_{h\%} = \frac{U_h}{U_1} \cdot 100\% \quad (3)$$

where U_h —rms of the h -th harmonic and U_1 —rms of the fundamental harmonic.

Additionally, the total harmonic distortion factor (THD) is often used. It characterizes the ratio of harmonic voltages generated by a non-linear device to the fundamental harmonic voltage [16]:

$$THD_{\%} = \frac{\sqrt{\sum_{h=2}^{40} U_h^2}}{U_1} \quad (4)$$

When calculating the THD factor, odd harmonics are usually taken into account, although even harmonics with large jumps in loads, or incorrectly operating converters,

may occur. The maximum values of the *THD* factor are determined by the distribution network operator.

1.5. Voltage Dips

A voltage dip is a sudden reduction in the rms voltage in the power grid node, below a certain, specific limit value, usually by a few milliseconds [18]. It ends with the return of the voltage to its initial value or a value close to its initial value.

Figure 4 shows a voltage dip. U_c is a declared voltage which has the value of rated voltage U_n in low-voltage grids. U_{ref} corresponds to the value of voltage before a dip, and U_{prog} is the value of voltage at the start of the dip. The amplitude of the voltage dip is determined by U_z , and the residual voltage U_r is the minimum value of voltage during the dip. Duration of the voltage dip is marked as T_z . According to the European DISPOWER project, voltage dips are the most frequent and most troublesome of interruptions in low voltage receiving grids [16,18]. Most frequently, they are caused by short-circuits switching loads with high inrush currents and the variability of the power; non-linear loads are characterized by this. Voltage dips are usually caused by short-circuits which last very short, because of the rapid activation of protection systems. Voltage dips caused by switching high-power loads and inrush currents last much longer, that is, from one to several seconds, but have a smaller amplitude. Among the types of voltage dips are short supply interruptions, i.e., interruptions during which the value of the supply voltage is zero. In practice, often the part of the grid cut off from power supply contains some energy stored in different forms, so that during short power interruptions the voltage is not zero. The voltage dip phenomenon can lead to interruptions in the operation of equipment and cause large losses and damage to the equipment [21].

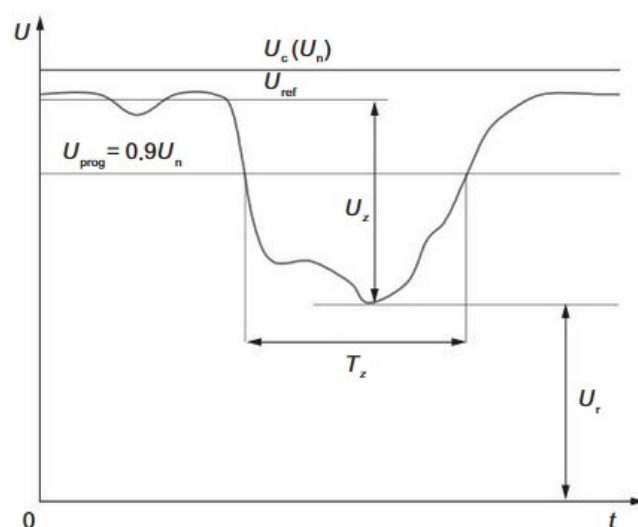


Figure 4. Graphic representation of a voltage dip [18].

1.6. Behaviour of Consumers That Reduces Voltage Fluctuations

An improvement in power supply quality can also be achieved by changing consumer behavior and habits. Various motivational strategies serve this purpose. This article [25] distinguishes four basic ones. The first one is to increase self-consumption. In Germany, for example, a special tariff has been introduced, regarding energy from photovoltaic sources in the immediate vicinity of the installation. By increasing the consumption of energy for their own purposes, the owner can make significant savings. Another solution is a tariff that takes into account changes in the energy price during the day. Energy prices depend on the availability and demand of energy at a given time. In order to facilitate a smooth supply, owing to energy price fluctuations, households and companies are encouraged to use energy when there is an excess of energy in the system. Such a situation usually occurs at night or during the midday hours. In addition to the variable costs of purchasing

electricity, the cost of electricity to the consumer also includes fees and taxes. The graph in Figure 5. shows an example of how energy prices fluctuate over time.

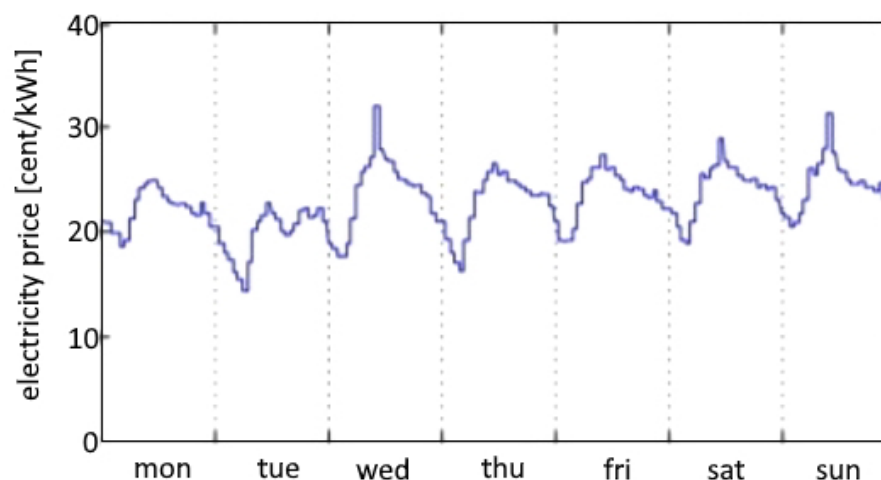


Figure 5. Changes in energy price over time [25].

Another motivational strategy to reduce power fluctuations at the household connection point and consequently also in the LV grid is to regulate the base energy price according to power. The base electricity price varies linearly throughout the day. In many countries, prosumers have the possibility to choose the most favorable tariff for their needs and energy consumption profile.

It is also worth noting solutions in which electric vehicles connected to the charging infrastructure constitute an energy reservoir, mitigating the daily fluctuations in the availability of energy generated in PV installations [4].

1.7. Overview of Global PV Systems

Research is continually being conducted to both improve the efficiency of PV installations and improve their interaction with the power system [26]. The increase in global generation of energy from photovoltaics systems is also being achieved through the development of the PV sector in developing countries characterized by good irradiance parameters. Such countries include Brazil [27], Afghanistan, Algeria [28] and India [29]. The performance of the installation can be increased by improving the PV modules themselves, minimizing the energy capture losses, which includes ensuring an adequate operating temperature of the installation and selection of appropriate inverters, protections and cabling. A key factor for improving interaction of the installation with the grid is the continuous monitoring of the amount of electricity generated and transmitted to the network along with forecasting energy generation and consumption, in order to avoid sudden voltage fluctuations and situations where the system becomes overloaded.

2. Materials and Methods

A model of a photovoltaic system connected to the power grid design objective. The performance analysis of the on-grid photovoltaic system was conducted using the Matlab/Simulink program. One example of a 100 kW photovoltaic power plant, connected to a 25 kV grid (“Detailed Model of a 100 kW Grid-Connected PV Array”) was used in this paper [30]. It comes from Matlab resources and is publicly available on the Mathworks platform. The aforementioned model was adapted to the needs of this paper. The power of the installation was reduced (to 12.2, 19.825 and 39.65 kW), the parameters of the power and electrical equipment were adjusted, the network voltage was changed to 20 kV, and the time-varying irradiance values measured on the Polish territory in Strzyżów, Podkarpackie Province, were implemented.

2.1. Description of the Model of the System with the On-Grid Photovoltaic Installation

The power system analyzed is shown in Figure 6. It consists of a PV module installation, a DC–DC boost converter, a three-phase voltage source controller (VSC), a capacitor bank to filter the harmonics generated by the VSC and a three-phase coupling transformer, as well as the power system [31].

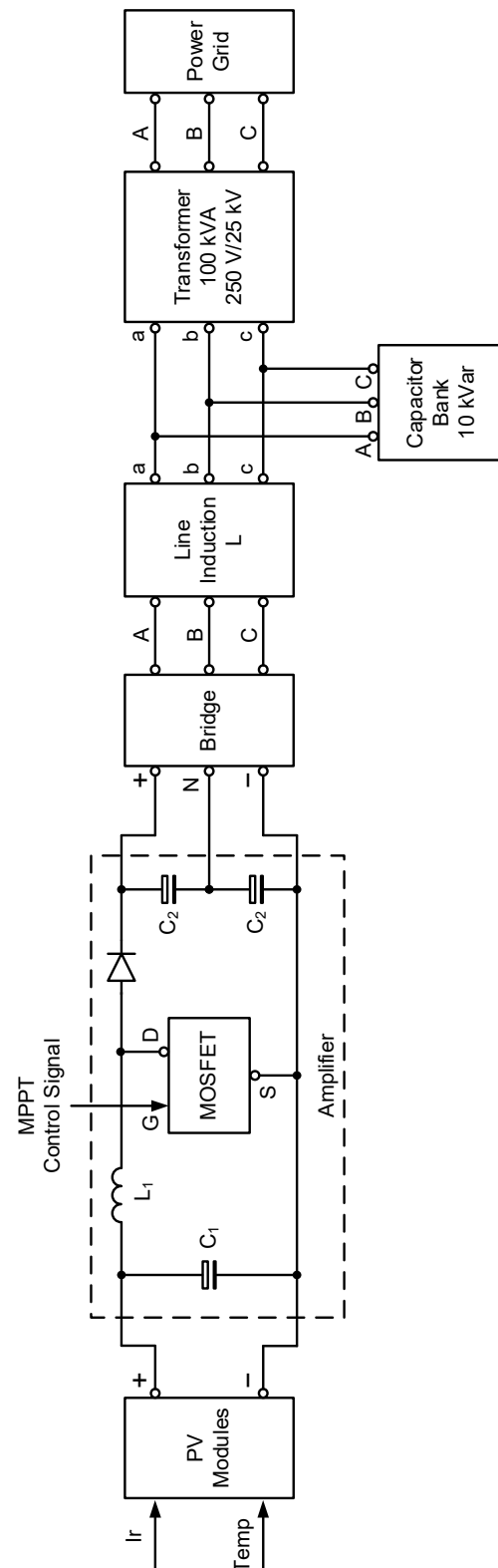


Figure 6. Diagram of the on-grid photovoltaic installation model implemented in Matlab/Simulink.

A simplified block diagram of the system [32], presenting the stages of energy conversion is shown in Figure 7.

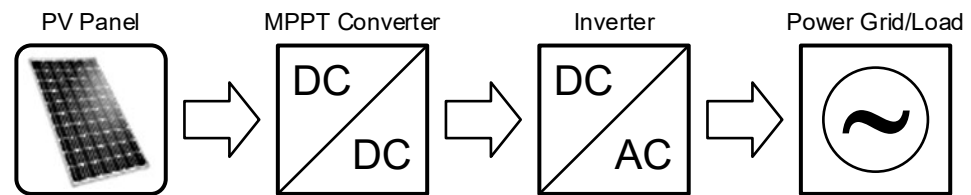


Figure 7. Block diagram of the energy conversion system.

The DC–DC boost converter, increases the DC input voltage coming from the photovoltaic modules to an output value of 500 V. The boost converter consists of a diode, a MOSFET transistor, which acts as a switch that closes and opens the circuit, as well as reactance elements that store energy—a coil and capacitors. In order to minimize the output voltage distortions, a low-pass filter was also used. The duty cycle of the converter is optimized by the MPPT regulator, so as to generate the voltage that would allow the maximum power value to be obtained. The voltage signal is regulated by means of Pulse Width Modulation (PWM). A fragment of the system showing a DC–DC converter together with a three-phase rectifier bridge, connected to a voltage source such as PV modules, is shown in Figure 8 and was implemented in the Matlab/Simulink program.

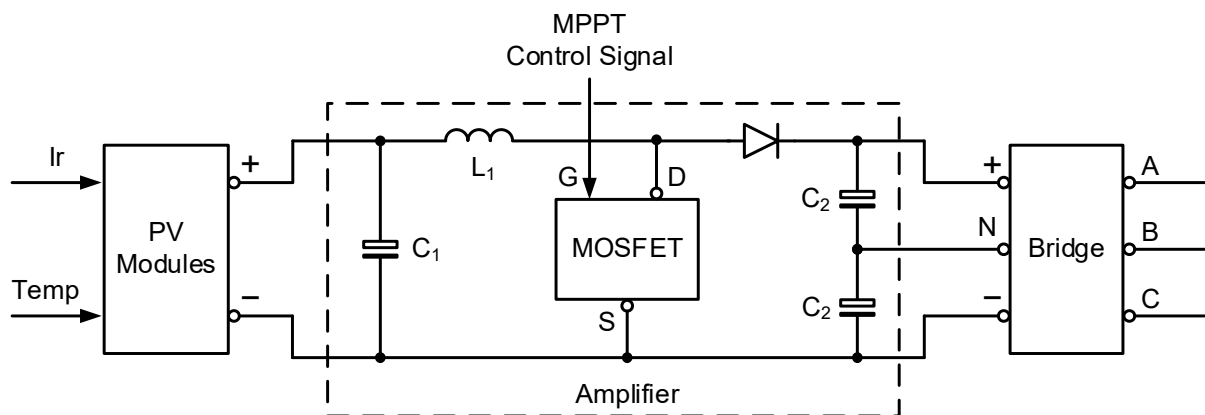


Figure 8. DC–DC boost converter together with a three-phase rectifier bridge, connected to a PV installation, implemented in Matlab/Simulink.

The three-phase, three-level VSC inverter, whose diagram was implemented in Matlab, is shown in Figure 9 and has the task of converting the DC voltage coming from the photovoltaic modules, boosted by the DC–DC converter to a value of 500 V, into 230 V AC voltage, compatible with the network voltage, as well as maintaining the power factor value within the set limits. It consists of a PLL, a DC voltage regulator, a current regulator and a PWM generator. The PLL is a phase synchronization loop, otherwise known as a phase-locked loop. It is an electronic circuit that works on the basis of the feedback principle and is used for frequency regulation. Its most important components include a low-pass filter, a phase detector and a voltage-controlled oscillator (VCO). The DC voltage regulator is a system whose role is the automatic maintenance of the set voltage level [33].

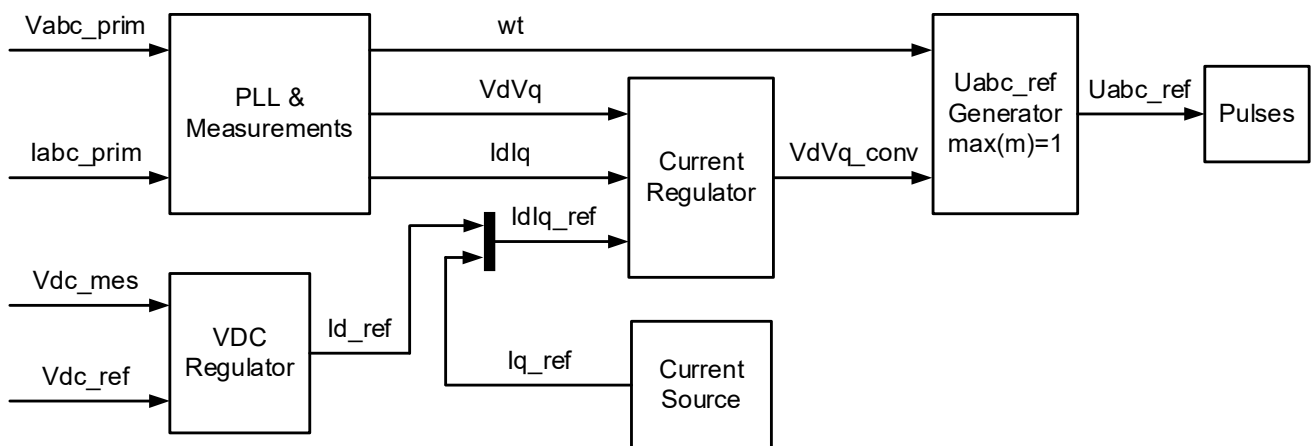


Figure 9. Diagram of the VSC inverter implemented in Matlab/Simulink.

The VSC system takes advantage of two control loops. The external loop regulates the indirect circuit voltage up to ± 230 V. The internal control loop regulates the parameters of components of the active and reactive components of the mains currents I_d and I_q . The set value of the active component I_d is equal to the current at the output of the voltage source controller. The reference value of the reactive component I_q is assumed to be equal to zero in order to maintain the power factor $\cos\phi = 1$. The voltage outputs V_d and V_q of the current controller are converted into three modulation signals, which are then supplied to the PWM generator.

Another component of the system is a capacitor bank with a reactive power of 10 kvar. Its task is to compensate the reactive power and filter the higher harmonics produced by the VSC. The operation of the battery is based on automatic switching on and off of individual capacitor modules of a specified size at the compensated point of the system. The reactive power regulator compares the current value of the power factor $\cos\phi$ with the preset value and selects the value of the capacitor bank in such a way as to continuously optimize $\cos\phi$ in the grid. In the case under consideration, the whole capacity of the capacitor bank is switched on. The device which connects the analyzed micro-installation with the power grid is a 100 kVA 230 V/20 kV three-phase transformer.

The power system is shown in Figure 10. It consists of a power line with a total length of 19 km and a voltage of 20 kV, resistive and resistive-inductive loads, a grounding transformer and a three-phase transformer increasing the voltage to 120 kV in the transmission lines. This model was implemented in the Matlab/Simulink program.

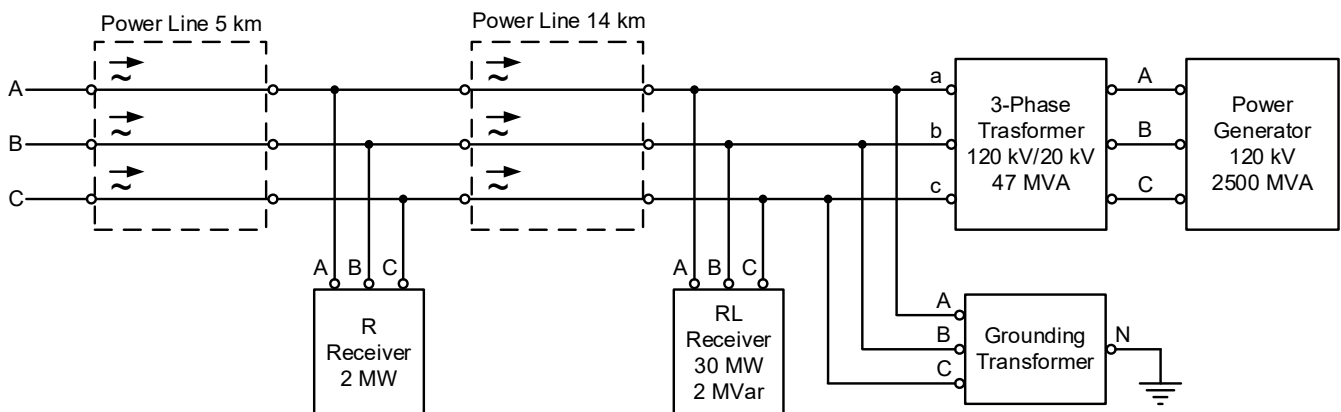


Figure 10. Diagram of the power system implemented in Matlab/Simulink.

The on-grid PV system model also includes a measurement system to measure the average power generated by the PV modules (Figure 11), a system to measure the voltage

and current on the modules (Figure 12), a system to indicate the values of the active and reactive component of the current in the VSC (Figure 13) and a system to visualize the operation of the maximum power point (MPPT) tracking algorithm (Figure 14).

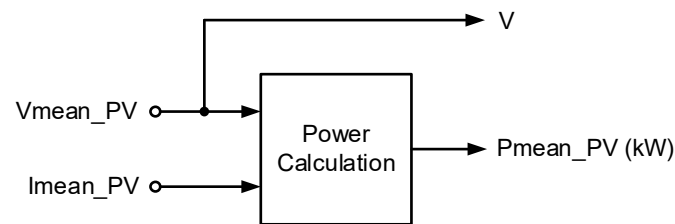


Figure 11. Diagram of the measuring system of the power of photovoltaic modules implemented in Matlab/Simulink.

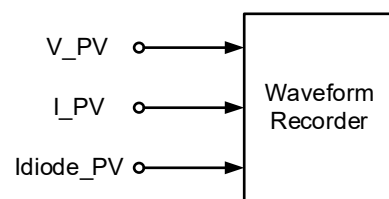


Figure 12. Diagram of the measuring system of parameters of photovoltaic modules implemented in Matlab/Simulink.

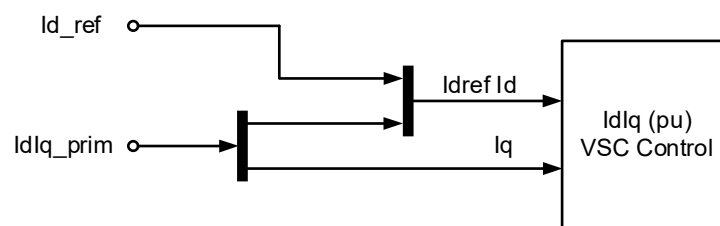


Figure 13. Diagram of the measuring system of the active and reactive component of the VSC current implemented in Matlab/Simulink.

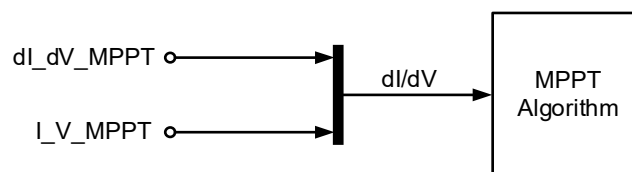


Figure 14. The system for the visualization of the operation of the maximum power point tracking (MPPT) algorithm implemented in Matlab/ Simulink.

The photovoltaic installation consists of SunPower SPR-305E-WHT-D panels [34] connected in chains. Depending on the analyzed case, their number is selected so as to obtain the pre-set energy generation.

For the selected model of photovoltaic modules, curves showing the relationship between power and current vs. voltage (Figure 15) were plotted in the Matlab program, depending on the irradiance and temperature values of the cells.

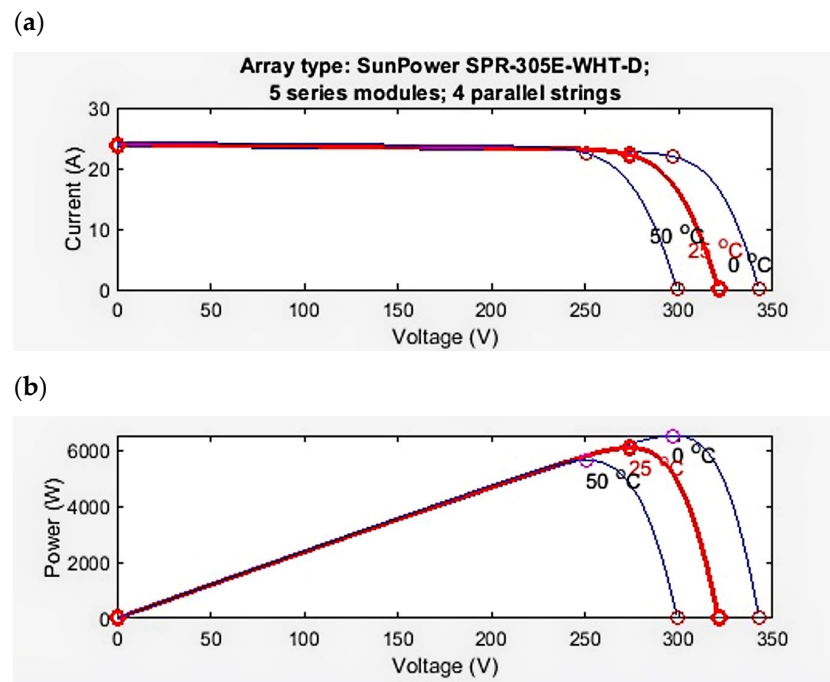


Figure 15. Curves showing the relationship between current (a) and power (b) and voltage, depending on irradiance and cell temperature, generated in Matlab/Simulink.

2.2. Input Data for Simulation

The operation of photovoltaic installations with three different powers was simulated. The irradiance measurements were made in Strzyżów, a town near Rzeszów in south-eastern Poland. This location is characterised by relatively good insolation conditions in comparison with other areas of the country. For the purpose of this paper, measurements from a sample day in July were analyzed as they best illustrate the investigated problem due to relatively high irradiance values.

The daily distribution of irradiance on the analyzed day is presented in the diagram (Figure 16). It can be noticed that during the night hours, without sunshine, the irradiance is equal to zero. On 18 July, already at approximately 6:00 a.m., the value of irradiance exceeds zero and remains positive until approximately 7:00 pm. The highest values of irradiance are observed between 10:00 a.m. and 3:00 p.m. In the graph showing the irradiance pattern for the July day, a clear decrease in values can be observed between 10:30 a.m. and 12:00 a.m., which is due to the temporarily cloudy weather and consequent lack of insolation of the modules. The highest measured values are equal to 1034 W/m^2 at 10:02 and 1026 W/m^2 at 11:48 a.m. The average irradiance value on 18 July 2021 was 263.9 W/m^2 .

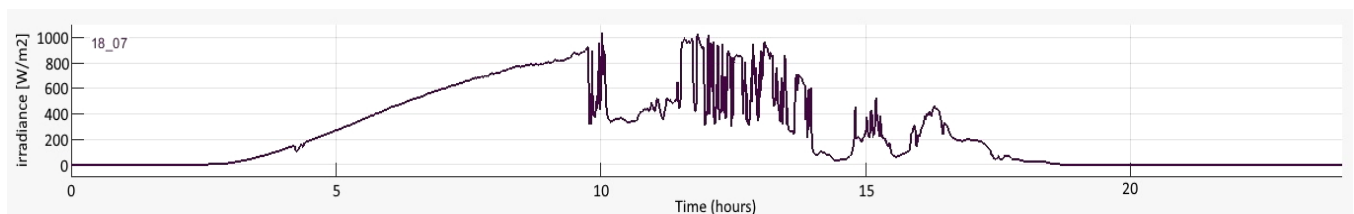


Figure 16. Daily distribution of irradiance on a sample day in July.

Solar cells, as semiconductor devices, are sensitive to temperature. Due to the lack of access to accurate measurement data, the temperature of the modules during system operation was estimated based on the literature and consultation with people involved in photovoltaic module research. The theoretical limit values for the operation of the selected PV modules range between $40 \text{ }^\circ\text{C}$ and $80 \text{ }^\circ\text{C}$. The optimum operating temperatures range

between 20 °C and 25 °C. According to the module data sheet [34], the current temperature coefficient is equal to 0.057%/°C; thus, as the temperature increases, the short-circuit current increases and the open circuit voltage decreases (the voltage temperature coefficient is $-0.27\%/^{\circ}\text{C}$). This means that as the temperature of the modules increases, the efficiency of energy generation decreases.

Each of the analyzed installations consists of parallel chains, each with five serially connected SunPower SPR-305E-WHT-D mono-crystalline modules (each module—305 W). The simulations are performed for installations consisting of:

A total of 8 strings of 5 panels each (the power of micro-installations—12.2 kW),

A total of 13 strings of 5 panels each (the power of micro-installations—19.825 kW), and

A total of 26 strings of 5 panels each (the power of micro-installations—39.65 kW).

In this paper, the current and voltage on the modules and the diode current, the power generated by the modules, as well as the momentary power and the voltage and current in the power system are analyzed. The simulation results are presented in Section 3.

3. Results and Discussion—Simulation of the Interaction of the PV Micro-Installation with the Power System

3.1. Simulation of the Operation of Photovoltaic Installations, Viz. the Power and the Average Voltage from the Output of the Modules

The average power generated by the modules and the average voltage at the output of the modules were simulated first. The simulation results for the individual installation powers are presented in the graphs in Figures 17–19.

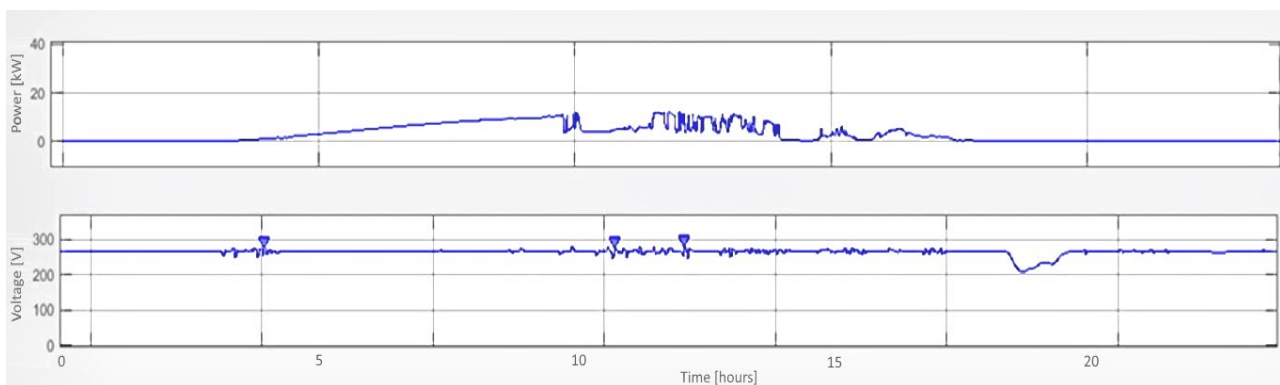


Figure 17. Daily waveform of power and the average voltage at the output of the PV modules (12.2 kW) on a sample day in July.

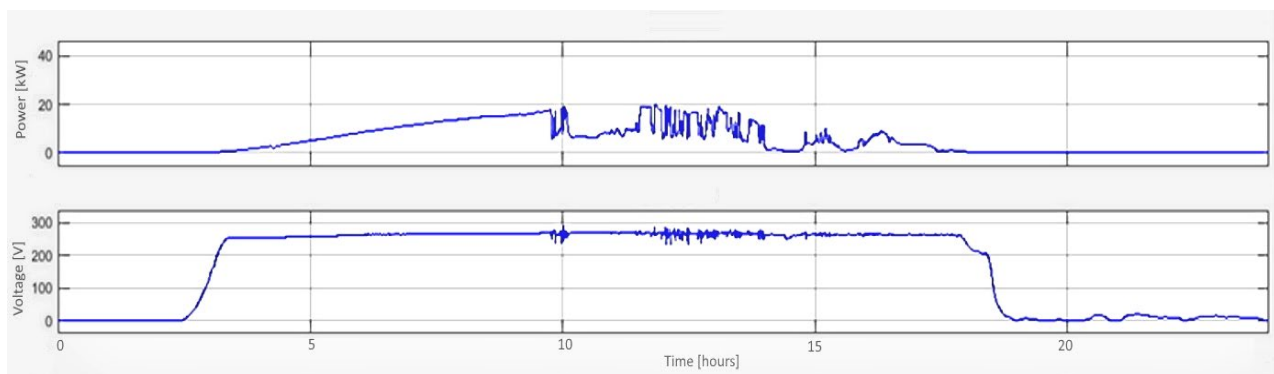


Figure 18. Daily waveform of power generated by the modules and the average voltage at the output of the PV modules (19.825 kW) on a sample day in July.

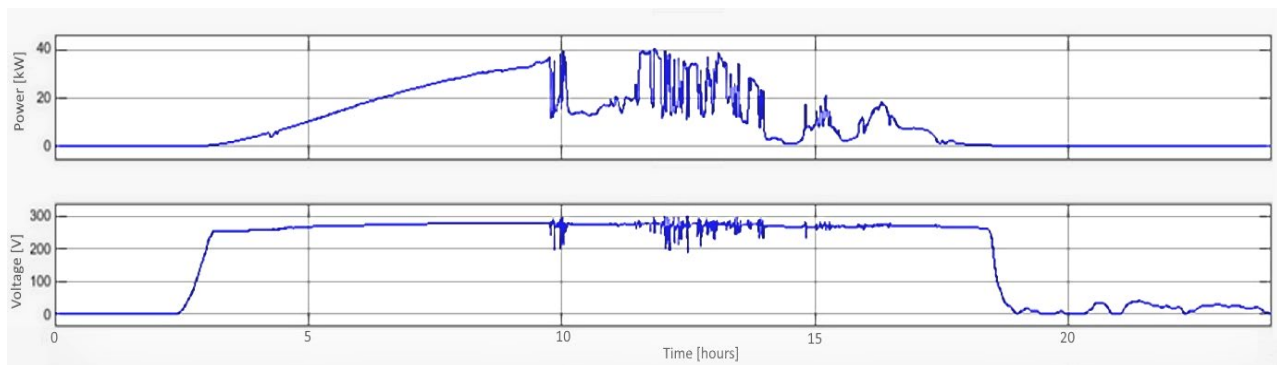


Figure 19. Daily waveform of power generated by the modules and the average voltage at the output of the PV modules (39.65 kW) on a sample day in July.

- Simulation on an exemplary July day for an installation (12.2 kW) comprising 8 strings of 5 panels, 305 W each.
- Simulation on a sample day in July for an installation (19.825 kW) comprising 13 strings of 5 panels, 305 W each.
- Simulation on a sample day in July for an installation (39.65 kW) comprising 26 strings of 5 panels, 305 W each.

The theoretical maximum power generated by the installation can be calculated from the following formula [19]:

$$P_{max} = P \cdot Z \cdot N \quad (5)$$

where P —power of a single module; Z —number of chains; N —number of modules in a chain.

For example, for an installation consisting of 26 chains, each with 5·305 W modules:

$$P_{max} = 305 \cdot 26 \cdot 5 = 39.65 \text{ kW}$$

However, the simulations were not conducted under STC conditions (irradiance = 1000 W/m², module temperature = 25 °C). For this reason, the actual power generated differs significantly from the theoretical values. These differences are most evident during the winter months, when the average irradiance is even 10-fold lower than under STC conditions. Table 1 shows a comparison between the theoretical values of the power that should be generated and the values obtained in the simulations.

Table 1. Values of the power P_{sr_max} generated by photovoltaic installations obtained in simulations and calculations.

Date	Number of Chains Containing 5 Modules Each, with a Power of 305 W Each	Theoretical P_{max} [kW]	Theoretical P_{sr_max} [kW]
18 July 2021	8	12.20	12.30
	13	19.83	19.96
	26	39.65	38.90

It can be observed that the maximum momentary power values obtained from the simulated operation of the installation in Simulink reach values close to the maximum theoretical power. This is due to the good conditions of the irradiance, which at its peak time, at 10:02 a.m., was 1034 W/m².

Then, the values of I_{PV} current and U_{PV} voltage on photovoltaic modules, as well as the current on I_{PV} diode, were simulated. The simulation results are presented in the graphs (Figures 20–22), generated in the Simulink program, and in Tables 2–4.

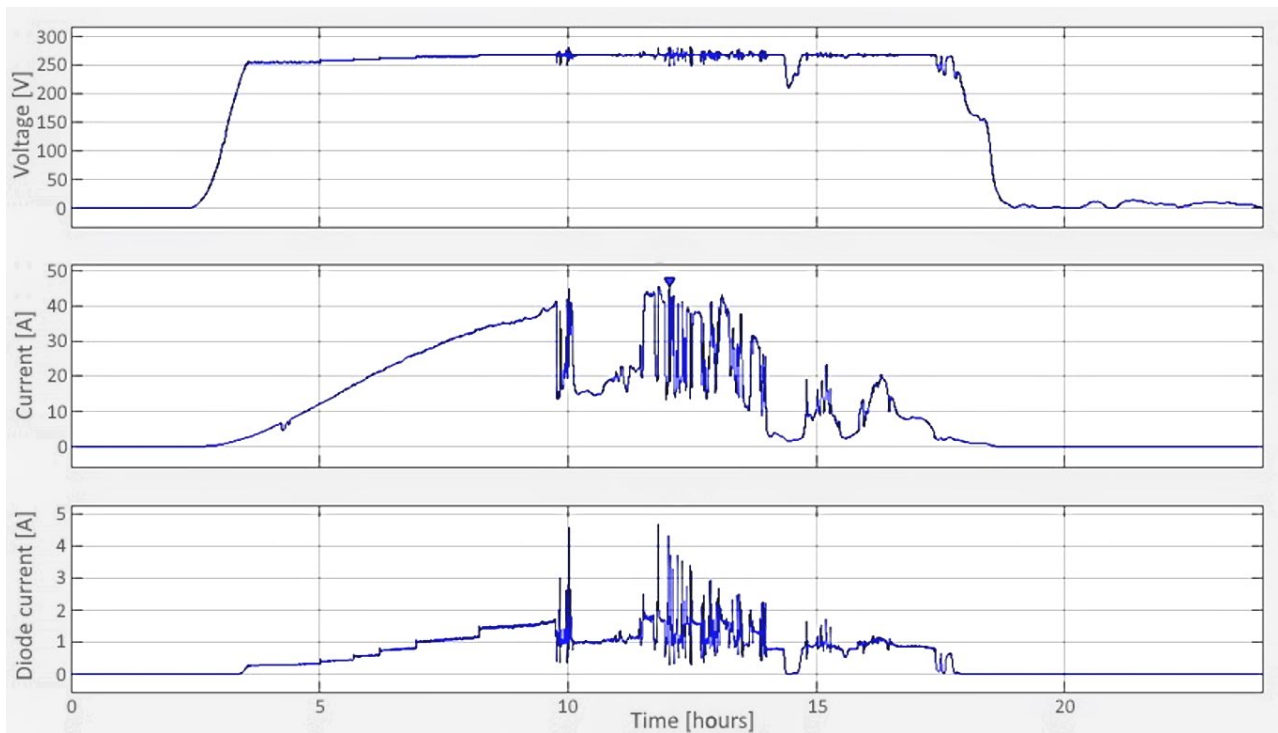


Figure 20. Daily waveforms of voltage and current of the PV modules (12.2 kW) and PV diode current on a sample day in July.

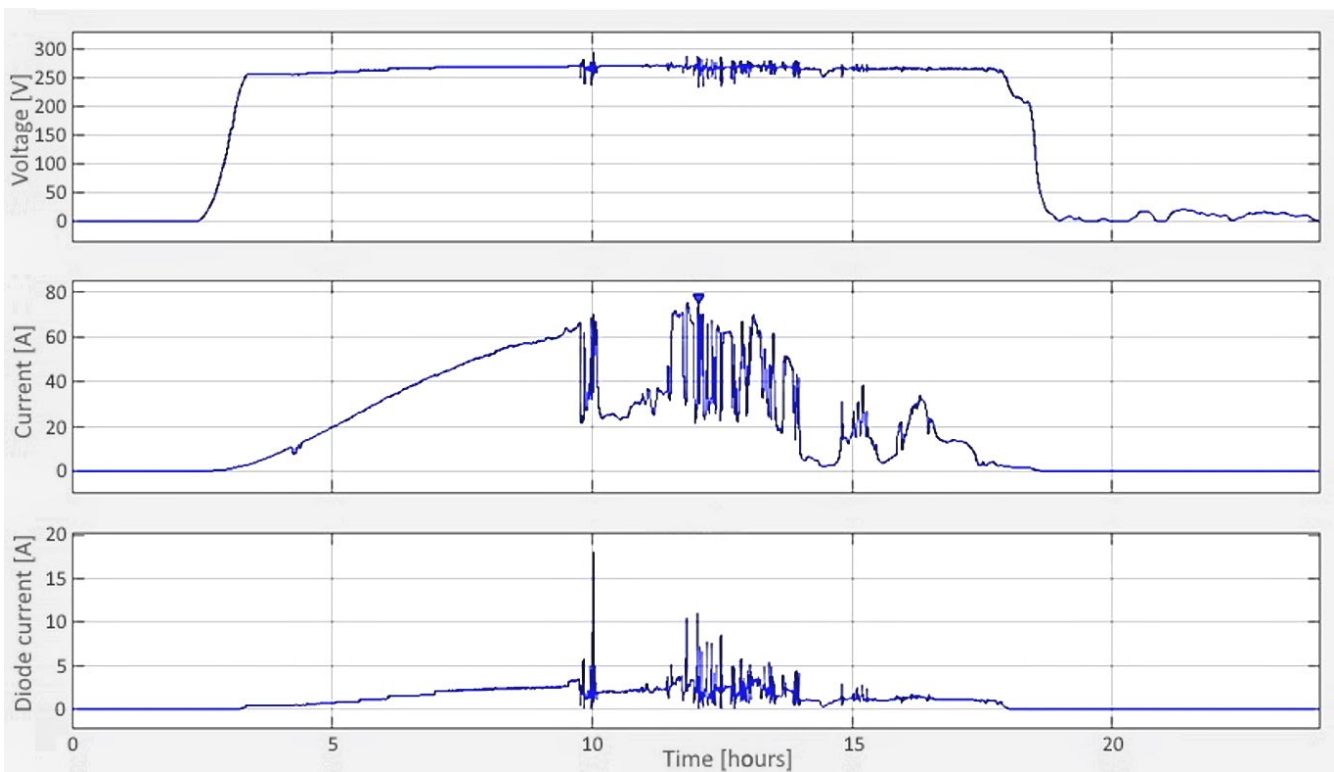


Figure 21. Daily waveforms of voltage and current of the PV modules (19.825 kW) and PV diode current on a sample day in July.

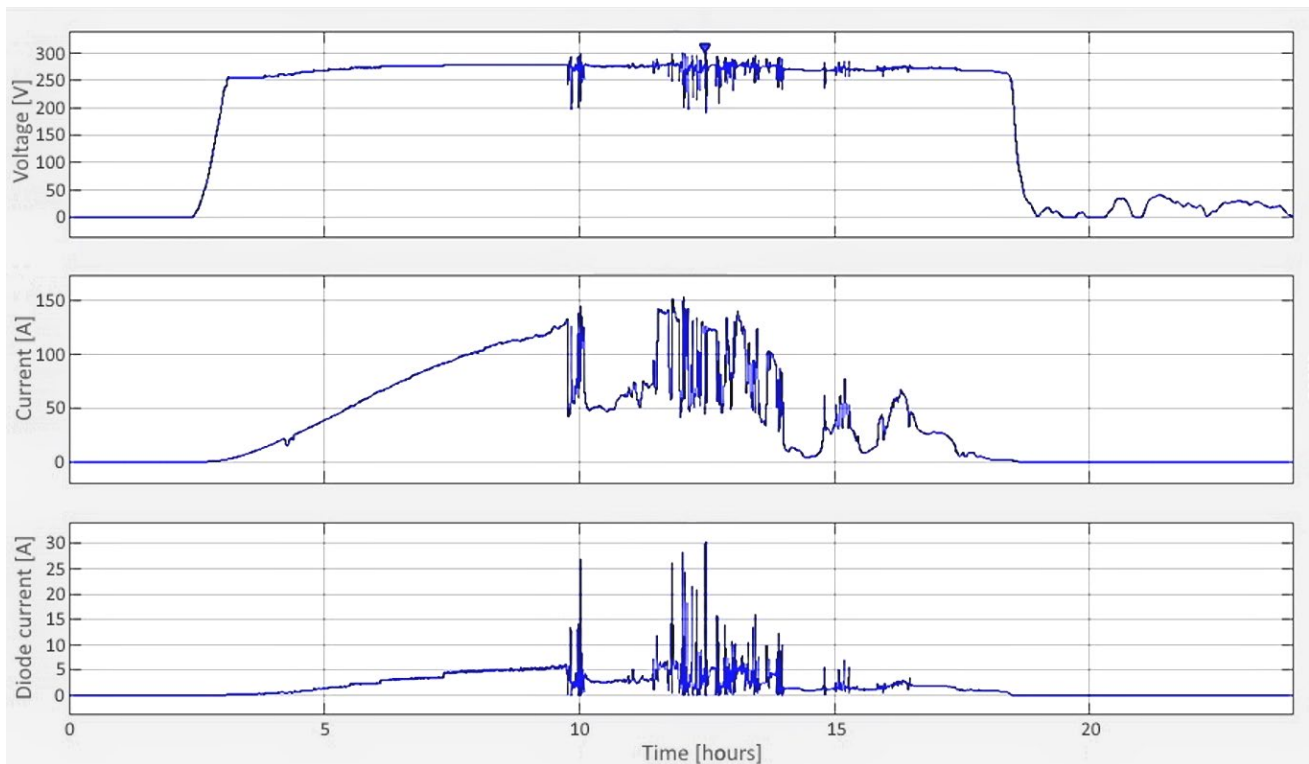


Figure 22. Daily waveforms of voltage and current of the PV modules (39.65 kW) and PV diode current on a sample day in July.

Table 2. Values of voltage and current on PV modules (12.2 kW) and PV diode current on a sample day in July.

Parameter	V_{sr} [V]	V_{PV} [V]	I_{PV} [A]	I_{diod_PV} [A]
Maximum value	281.8	282	45.87	4.698
Time of occurrence of the maximum value	12:26	12:26	12:03	11:44
Minimum value	0	0	$-5.996 \cdot 10^{-10}$	0
Time of occurrence of the minimum value			20:46	
Mean value	169.9	168.3	11.65	0.5695
Median	257.6	257.6	5.741	0.4144

Table 3. Values of voltage and current on PV modules (19.825 kW) and PV diode current on a sample day in July.

Parameter	V_{sr} [V]	V_{PV} [V]	I_{PV} [A]	I_{diod_PV} [A]
Maximum value	292.6	292.9	75.31	18.05
Time of occurrence of the maximum value	10:01	10:01	12:01	10:02
Minimum value	0	0	$-2 \cdot 10^{-10}$	0
Time of occurrence of the minimum value		172.7	20:48	
Mean value	172.7	260.2	18.84	1.011
Median	260.2		9.457	0.8382

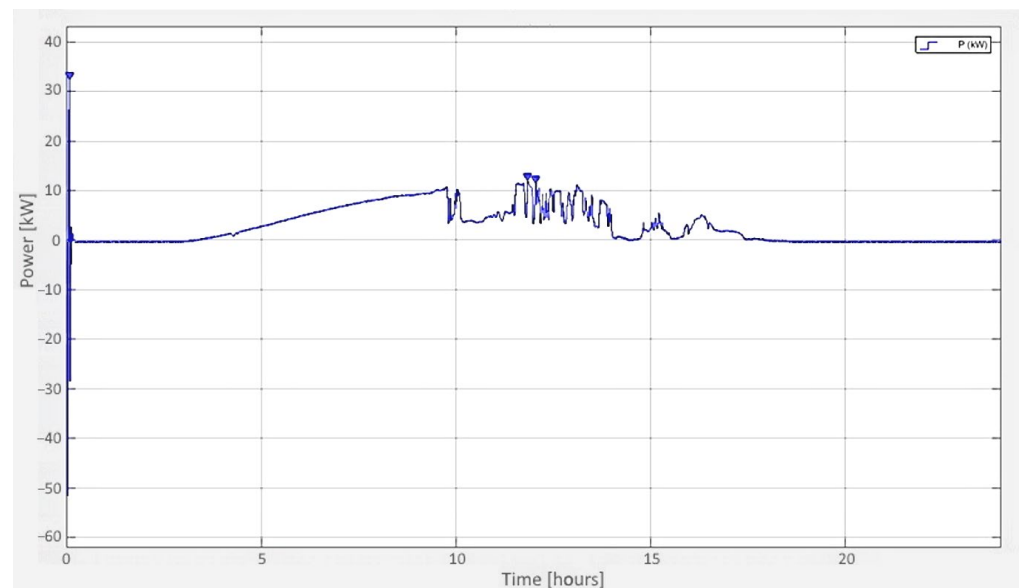
Table 4. Values of voltage and current on PV modules (39.65 kW) and PV diode current on a sample day in July.

Parameter	V_{sr} [V]	V_{PV} [V]	I_{PV} [A]	I_{diod_PV} [A]
Maximum value	293.2	301.6	154.5	31.67
Time of occurrence of the maximum value	12:28	12:27	12:03	12:27
Minimum value	0	0	$-8.71 \cdot 10^{-10}$	0
Time of occurrence of the minimum value	181.8	181.8	20:41	
Mean value	267.5	176.7	37.63	2.083
Median		260	19.05	1.325

- Simulation on a sample day in July for an installation (12.2 kW) comprising 8 strings of 5 panels, 305 W each.
- Simulation on a sample day in July for an installation (19.825 kW) comprising 13 strings of 5 panels, 305 W each.
- Simulation on a sample day in July for an installation (39.65 kW) comprising 26 strings of 5 panels, 305 W each.

3.2. Simulations of the Parameters of the Power Grid

Simulations of the values of the power P_B1 currently supplied to the grid by the photovoltaic installation and the values of the current and voltage of the power grid were also performed. The results are presented in the graphs in Figures 23–25.

**Figure 23.** Daily waveform of the power supplied (12.2 kW) to the network on an exemplary day in July.

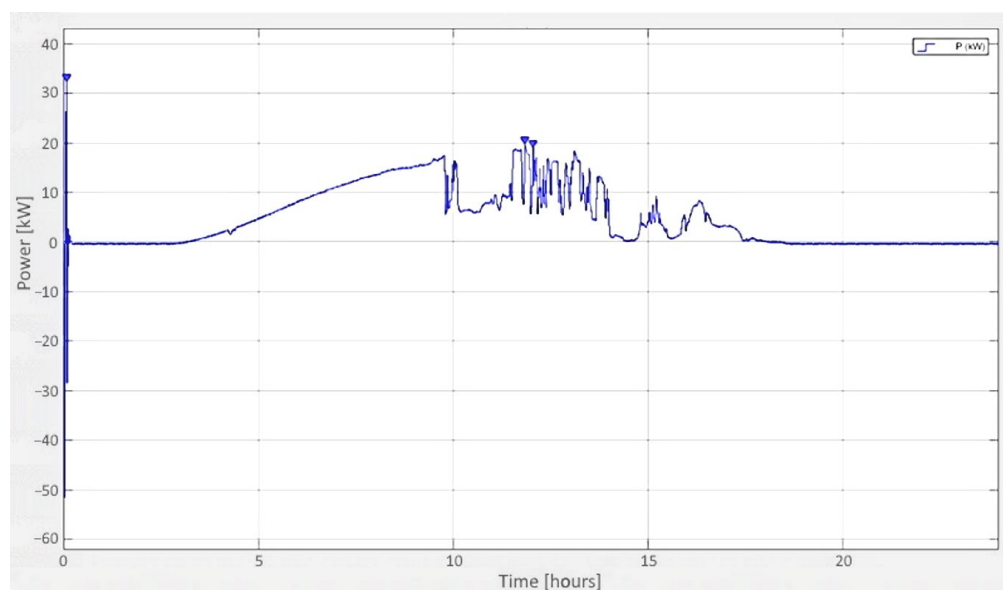


Figure 24. Daily waveform of the power supplied (19.825 kW) to the network on a sample day in July.

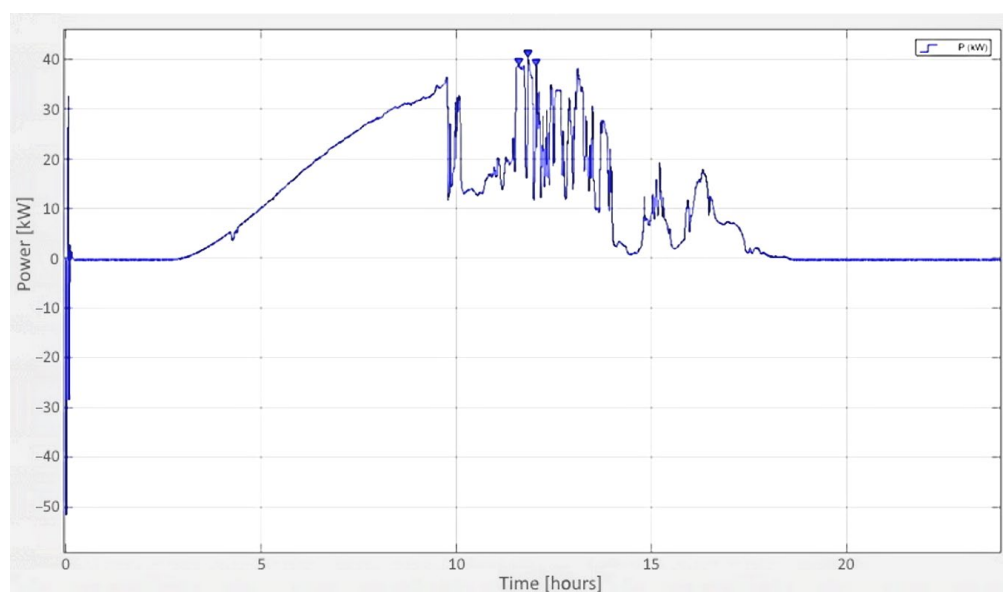


Figure 25. Daily waveform of the power supplied (39.65 kW) to the network on an exemplary day in July.

- (a) Simulation on a sample day in July for an installation (12.2 kW) comprising 8 strings of 5 panels, 305 W each.
- (b) Simulation on a sample day in July for an installation (19.825 kW) comprising 13 strings of 5 panels, 305 W each.
- (c) Simulation on a sample day in July for an installation (39.65 kW) comprising 26 strings of 5 panels, 305 W each.

The power P_{B1} is supplied to the network just after it is generated in the photovoltaic installation. It can be noted that the waveform of the power supplied during the day is very close to the daily irradiance waveform. This confirms the fact that the power generated directly depends on the irradiance. At the beginning of the simulation, power fluctuations of high amplitude are observed. After a while, they stabilize. They are an error of the simulation. On 18 July, the power is delivered to the grid between 4:30 a.m. and 7:45 p.m. Due to the cloudy weather and reduced irradiance, a smaller amount of energy supplied

to the grid is observed around 10:00 a.m. The maximum, instantaneous value of power, supplied to the power system on the July day under analysis by the 39.65 W installation was 38.64 kW. This value was recorded at 11:51. This is 1 kW less than the value generated by the PV installation. This may be due to losses in the wires, as well as inaccurate selection of the parameters of the equipment.

A simulation of the waveform of voltage V_a and current I_a of phase A in the power system was also performed. It was assumed that the phase load is symmetrical, which means that the simulation results for each phase will be identical. The simulation was performed for a sample day in July for an installation (39.65 kW) comprising 26 strings of 5 panels, 305 W each. The results presented in graphs (Figures 26 and 27) refer to the installation consisting of 26 strings of 5 panels, 305 W each.

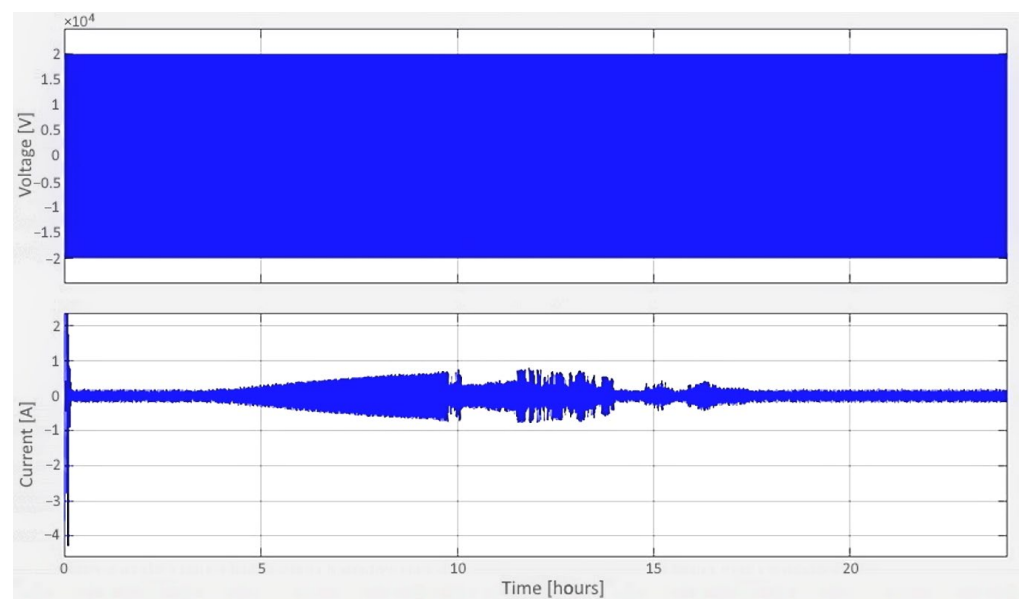


Figure 26. Daily waveforms of voltage and current in the grid, phase A on a sample day in July.

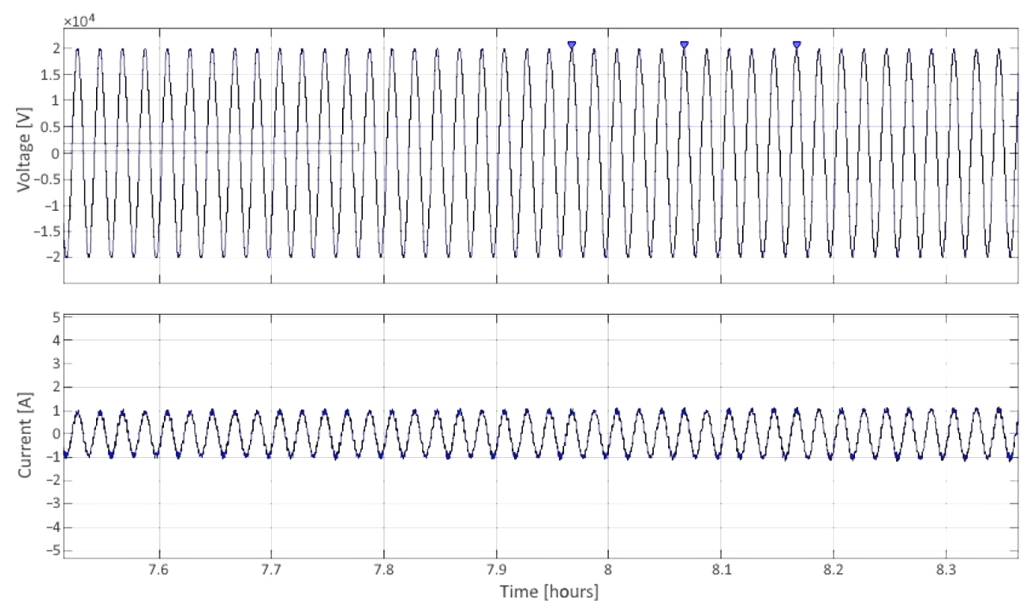


Figure 27. Approximation of the waveforms of voltage and current in the network, phase A, on a sample day in July day between 7:30 a.m. and 8:30 a.m.

Only the graphs for an installation (39.65 kW) consisting of 26 strings with 5 modules of 305 W each were presented. Only the graphs for such an installation were included,

as the graphs for installations with lower powers follow the same waveform. For the remaining installations, the maximum and minimum values of current I_a and voltage V_a in the network are presented in Table 5.

Table 5. Maximum and minimum values of current and voltage of the power system.

Date	Number of Chains with 5 Modules Each, with a Power of 305 W Each	V_{a_max} [kV]	V_{a_min} [kV]	I_{a_max} [A]	I_{a_min} [A]
18 July 2021	8	19.91	−19.93	4.078	−4.287
	13	19.90	−19.89	4.078	−4.287
	26	19.91	−19.93	4.078	−4.287

It can be observed that the current and voltage have a sinusoidal waveform. The theoretical voltage of the power system at the point of connection of the installation to the grid assumed in this paper is 20 kV. The obtained values are slightly lower. This is due both to the inaccuracy of the simulation and to the inaccurately selected values of the installation components. No local voltage peaks are observed, which could be influenced by the connection of the photovoltaic installation to the network.

The current waveform I_a reaches its highest amplitudes when the installation is switched on. The highest value that it reaches is 4.078 A. Then, its values stabilise at ± 0.25 A. As the sun rises and the irradiance, and therefore the power generated by the photovoltaic installation increases, so does the amplitude. In the afternoon and evening, as the insolation decreases, the current amplitudes decrease. After the sunset, when the irradiance becomes zero, the amplitude of the current value remains equal to approximately 0.5 A. In the case under consideration, a simplification was made, that the components of the power system are symmetrical and linear, and the different phases operate under the same load. Therefore, it was assumed that the current and voltage in phases A, B and C have identical values.

3.3. Discussion of the Simulation Results Obtained for the 39.65 kW Installation

A photovoltaic installation consisting of 26 strings, 5 modules of 305 W each, was analyzed in detail. Its maximum theoretical power under STC conditions is 39.65 kW.

The rated data of the SunPower SPR-305E-WHT-D panels were read from the data sheet [34]:

Open circuit voltage: $V_{oc} = 64.2$ V,

Voltage at maximum power point: $V_{mp} = 54.7$ V,

Short-circuit current: $I_{sc} = 5.96$ A,

Current at maximum power point: $I_{mp} = 5.58$ A, and

NOCT (Nominal Operating Cell Temperature) = 46 °C.

For the selected panels, the most important operating parameters were calculated and compared with the values obtained by simulation in Matlab/Simulink.

(a) Voltage variations [29]:

Voltage temperature coefficient $\alpha = -0.27\%/^{\circ}\text{C}$

$$\Delta U_{1^{\circ}\text{C}} = |\alpha| \cdot V_{oc} = 0.0027 \cdot 64.2 = 0.17334 \text{ V} \quad (6)$$

where $\Delta U_{1^{\circ}\text{C}}$ —voltage change per 1 °C, V_{oc} —open circuit voltage [V], and α —voltage temperature coefficient.

(b) Open circuit voltage V_{oc}

The maximum voltage on the cells would occur, if the circuit was open and would then be [19,29]:

$$V_{oc} = V_{oc} \cdot N = 64.2 \cdot 5 = 321 \text{ V} \quad (7)$$

In the case under consideration, the condition when the circuit is open and the maximum voltage present on the PV cells is equal to 301.6 V is not observed. This value was read from the graph showing the relationship between the average voltage of the photovoltaic cells and time.

(c) Operating voltage V_r

During continuous operation, the installation operates at its operating voltage. This value can be calculated using the following formula [29]:

$$V_r = [V_{mp} - (\text{NOCT} - 25) \cdot \alpha] \cdot N = [54.7 - (46 - 25) \cdot 0.17334] \cdot 5 = 255.9 \text{ V} \quad (8)$$

where V_r —operating voltage [V], V_{mp} —voltage at the maximum power point, and N —number of modules per string

$$255.19 \text{ V} < 321 \text{ V}$$

The operating voltage takes a lower value than the open circuit voltage, which is consistent with the real situation.

(d) Low temperature operating voltage V_{r-low} [29]:

Minimum operating temperature = -40 °C.

$$V_{r-low} = [V_{mp} - (T_{min} - 25) \cdot \alpha] \cdot N = [54.7 - (-40 - 25) \cdot 0.17334] \cdot 5 = 329.84 \text{ V} \quad (9)$$

where V_{r-low} —low temperature operating voltage [V]; T_{min} —minimum operating temperature of modules [°C].

The highest possible voltage of the modules is observed at their minimum operating temperature.

(e) High temperature operating voltage V_{r-high} [29]:

Maximum module temperature = 80 °C.

$$V_{r-high} = [V_{mp} - (T_{max} - 25) \cdot \alpha] \cdot N = [54.7 - (80 - 25) \cdot 0.17334] \cdot 5 = 225.83 \text{ V} \quad (10)$$

where V_{r-high} —high temperature operating voltage [V]; T_{max} —maximum operating temperature of modules [°C] [21].

At the highest possible operating temperature of the cells, the operating voltage reaches much lower values than at the low operating temperature. These values differ by more than 100 V. This is due to the fact that the high temperature is a result of heating of the modules at high insolation and generation of high currents in them.

In the analyzed case, the highest operating temperature of the cells was 41 °C. According to the calculation based on Formula (10) the operating voltage $V_{r-41^\circ\text{C}}$ should then be 259.63 V [29].

$$V_{r-41^\circ\text{C}} = [V_{mp} - (T_{max} - 25) \cdot \alpha] \cdot N = [54.7 - (41 - 25) \cdot 0.17334] \cdot 5 = 259.63 \text{ V} \quad (11)$$

where $V_{r-41^\circ\text{C}}$ —voltage on modules at operating temperature equal to 41 °C [V].

The average voltage of the modules measured in the simulation is 293.2 V, so it is higher than the theoretical value by more than 30 V. However, it is within the limits of acceptable voltage of the modules which is 321 V.

$$259.63 \text{ V} < 321 \text{ V}$$

(f) Maximum power generated by the panels

DC link capacitors are charged to the voltage of $557.4 \text{ V} = V_{dc} = V_{ref} - V_{avg}$. This value can be read from the VSC graph (Figure 28) obtained in the simulation in Matlab.

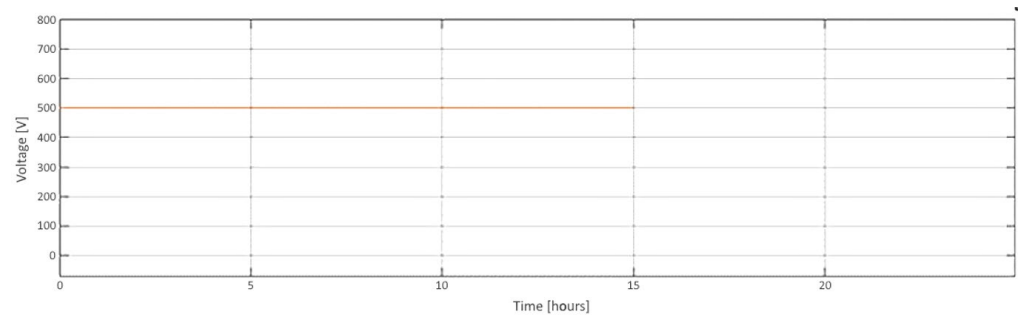


Figure 28. VSC inverter voltage graph.

The MPPT (Maximum Power Point Tracking) charge regulator is designed to control the voltage of V_{PV} modules by changing the duty cycle (D) to obtain the maximum power value P_{max} . From the MPPT graphs obtained in Matlab/Simulink (Figure 29), it can be read that the maximum power, equal to 38.9 kW, is generated by the modules when the duty cycle D is equal to 0.5235. The voltage of the modules is then equal to [19,29]:

$$V_{PV \text{ w MPP}} = (1 - D) \cdot V_{dc} = (1 - 0.5235) \cdot 557.4 = 265.6 \text{ V} \quad (12)$$

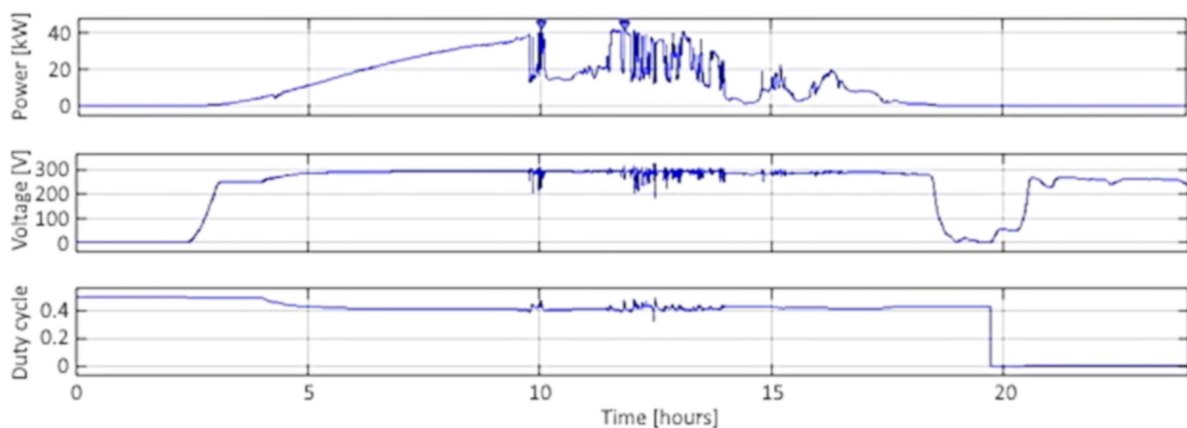


Figure 29. Graph of the power of photovoltaic modules and the average voltage across them and the duty cycle for a 39.65 kW installation on a sample day in July.

The maximum power obtained in the simulation at $D = 0.5235$ is 38.9 kW. The maximum theoretical power under STC conditions, according to Equation (13), is equal to 39.65 kW, so the values are similar [19]:

$$P_{max} = N \cdot Z \cdot P = 26 \cdot 5 \cdot 305 = 39.65 \text{ kW} \quad (13)$$

(g) Maximum, short-circuit current I_{sc} [19]:

$$I_{sc} = I_{sc1} \cdot Z = 5.96 \text{ A} \cdot 26 = 154.96 \text{ A} \quad (14)$$

where Z —number of chains; I_{sc1} —short-circuit current of a single module [A].

The value of the maximum short-circuit current I_{SC} measured in the simulation in the Simulink program is 154.5 A. Therefore, the theoretical value calculated by Formula (14) and the measured value are almost identical.

(h) Maximum operating current I_r [19]:

$$I_r = I_{mpp} \cdot Z = 5.58 \text{ A} \cdot 26 = 145.08 \text{ A} \quad (15)$$

where I_r —operating current [A], I_{mpp} —module current at maximum power point [A].

The maximum operating current permissible is 145.08 A. It takes a smaller value than the maximum short-circuits current, which is consistent with the real situation.

$$145.08 \text{ A} < 154.96 \text{ A}$$

(i) Current and voltage in the power system

On the graphs generated in Simulink in the GRID block it is possible to see the waveform of voltage and current on a 20 kV bus in one of the three phases, called phase A. As in previous simulations, a simplification was made, that the elements of the power system are symmetrical and linear, and the phases work under the same load. It follows that the current and voltage in phases B and C have the same values as in phase A. The voltage waveform throughout the day is constant and sinusoidal, oscillating between approximately 20 and -20 kV. The theoretical value of voltage V_a is equal to 20 kV, but the maximum value obtained in the simulation is 19.91 kV. The difference is extremely small. It is caused by local voltage drops and the influence of the photovoltaic installation connected to the network. The value of the I_a current in the power network oscillates around approximately $+/- 4.2$ A. The largest amplitudes are observed when the PV installation is connected to the grid. During the night hours, the amplitude stabilizes. From approximately 5:00 a.m., the amplitude increases as the irradiance increases and, consequently, the power generated from the PV installation increases. Between 10:00 and 12:00 a.m., when the weather is cloudy and the generated power decreases, the amplitudes of the I_a are much smaller. The values obtained in the simulations are presented in Table 6.

Table 6. Values of parameters of the PV installation on a sample day in July.

Parameter	P_{sr} [kW]	V_{sr} [V]	V_{PV} [V]	I_{PV} [A]	I_{diod_pv} [A]	P_{B1} [kW]	V_a [V]	I_a [A]
Maximum value	38.90	293.2	301.6	154.5	31.67	38.64	19,910	4.078
Time of occurrence of the maximum value	11:48	12:28	12:27	11:52	12:27	11:54		00:04
Minimum value	0	0	0	$-8.71 \cdot 10^{10}$	0	-51.5	$-19,930$	-4.287
Time of occurrence of the minimum value				8:41		00:06		00:07
Mean value	10.31	181.8	176.7	37.63	2.083	9.61		0.00083
Median	50.52	267.5	260	19.05	1.352	4.62		0.00079

4. Methods for Improving Power Quality

The intention of the authors, in this chapter, is to present the selected methods for improving the quality of power supplies, which are used in solving problems arising therein- during co-operation of the energy system with a larger number of distributed, PV micro-installations. The solutions presented in Sections 4.1 and 4.2 can be implemented in simulation tasks concerning, in particular, installations consisting of a larger number of PV micro-installations or small PV installations, in a small area of the power grid; this will be the subject of further research by the authors.

4.1. Compensating for Passive Power

Improving the quality of electricity and power supplies has always been an important issue in the functioning of a power system. In recent years, while saturation of the network with micro-installations of renewable sources has been growing rapidly, it becomes a key issue for the correct and stable operation of the system. Among the most common ways to improve power quality is passive power compensation. This provides a reduction in active power losses and harmful drops in voltage and allows network capacity to be increased. For this purpose, passive power compensators are used. These include parallel compensators: TCR/TSC (Thyristor Controlled Reactor/Thyristor Switched Capacitor)—Figure 30, FC/TCR (Fixed Capacitor/Thyristor Controlled Reactor)—Figure 31 and serial compensators such as SSC (Static Series Compensator)—Figure 32. Among the oldest methods is the use of capacitor

batteries, divided into stages, which makes it possible to adjust reactive power, step by step and adjust its value to the changing load. A more advanced solution, characterised by better operational dynamics and smaller size, albeit at much higher cost, is the STACOM system (Static Synchronous Compensator). This is a static source of AC voltage with an adjustable value and is used to improve the quality of the power supply in HV networks. Its most important part is the voltage inverter, built using thyristors and connected to the network by inductive reactance or a VSI voltage inverter (Voltage Source Inverter) with power transistors; it acts as a controlled voltage source.

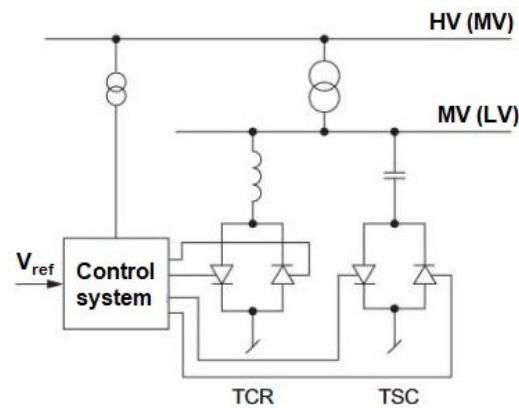


Figure 30. TCR/TSC compensator layout [35]: HV—high voltage, MV—medium voltage, LV—low voltage, and V_{ref} —reference voltage.

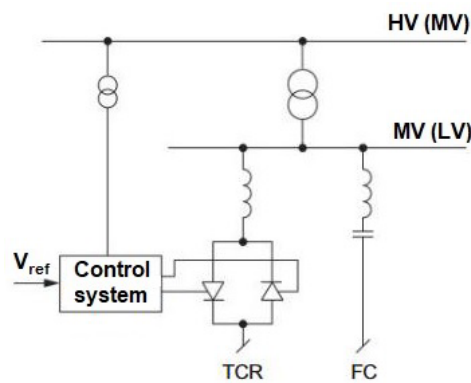


Figure 31. Schematic diagram of the static compensator system [35].

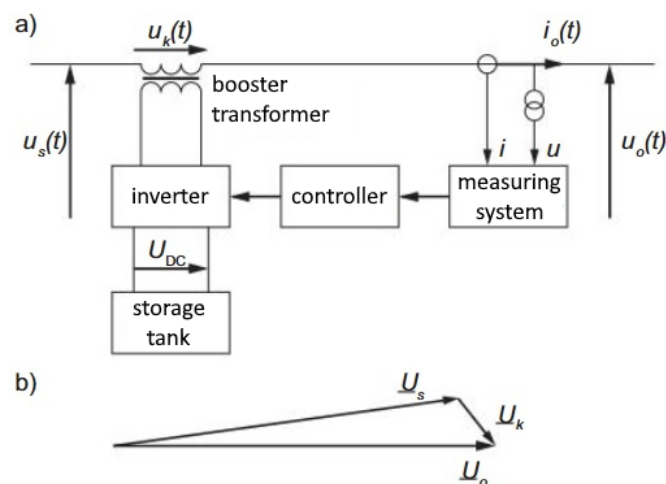


Figure 32. Series compensator [35]: (a) single-phase substitution diagram and (b) voltage indication diagram, where U_o —receiver voltage, U_z —mains voltage, and U_k —compensator voltage.

Where the SSC is designed to improve the quality of the voltage at the receiver terminals and compensate for voltage distortions and asymmetries of the supply network, it acts as a series active energy filter SAPF (Series Active Power Filter). In order to make the mains voltages symmetrical, it is necessary to eliminate the negative and zero sequence, symmetrical components. Filtering mains voltage distortions requires that the booster voltages include the same harmonics as the mains voltage, but with opposite phase angles.

4.2. Possibilities of Using Energy Storage to Improve Power Quality

Electric energy storage systems are systems that allow electricity to be collected, in any form, by converting it into another type of energy or storing it in a magnetic or electric field. Then—and upon demand—it can be processed and returned in the form of electricity with specific parameters. There are many types of electric energy storage, all differing in the form of energy storage, energy and power density and practical application. Many of these are used to improve the stability and the reliability of power systems. Energy storage systems with so-called significant capacity, which include pumped storage power plants and pneumatic energy storage facilities, are widely used. They make it possible to collect very large amounts of energy and also support energy management in power systems. Energy storage is also increasingly used in micro-installations, in distributed generation. Batteries and super-capacitors are used in this area. Batteries, or secondary electrochemical cells, store electrical energy in the form of chemical energy, thanks to the reversible chemical reactions taking place in them. There are many different types of batteries. Their common features include high energy density and low power density, an efficiency of up to 80% and a relatively low durability of 6–10 years. It is among the oldest and best developed technologies, allowing relatively low prices to be achieved. A major limitation is the strong dependence of capacitance, durability, EMF and internal resistance to temperature, as well as sensitivity to deep discharge. Supercapacitors are another solution used; these are electrolytic capacitors.

Their work consists in accumulating electric charges in the area of the electric double layer, formed at the boundary of the electrode and the electrolyte, as shown in Figure 33. They are characterized by a very high electrical capacity and power density, which gives them the ability to consume a large amount of energy, in a short time, and thus the possibility of charging and discharging with very high currents. Supercapacitors also have low, internal resistance, which means relatively few internal losses. Their great advantage is also their great efficiency, reaching 98%, and their high durability. The biggest obstacle to using this type of energy storage is its very high price.

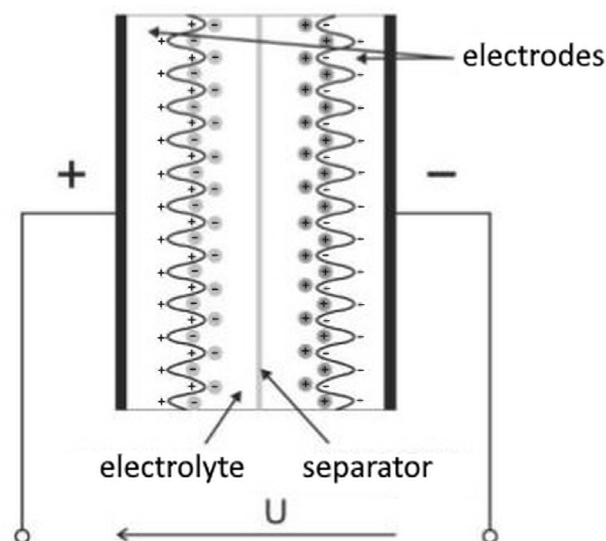


Figure 33. Formation of double layers in a charged supercapacitor [36].

Depending on the type and parameters, energy storage devices are used in various power operation systems. These applications can be divided into two basic groups:

- Support in the management of active energy, in normal network operation;
- Support for the power supply of receivers during interruptions to the supply network.

The first category includes increasing the connection capacity of the distribution network by reducing peak loads and also by balancing loads, or equalizing. This allows the reliability of the power supply to be increased and also has an impact on reducing power and energy losses in the network. In micro-installations, when the generating source is in operation for local needs, the use of energy storage allows energy to be accumulated when an excess is produced and used later, when needed. This allows energy consumption from the supply grid to be significantly reduced. Energy storage also acts as a compensator, allowing changes, in the generated power, delivered to the grid, to be limited. The task of supporting the power supply of consumers is best fulfilled by high-density, energy storage with a short response time; furthermore, those systems with lengthy charging and discharging times, such as accumulator batteries, work best as storage facilities. Devices used as energy sources in the event of interruptions to power in the grid, should be characterized by a discharge time of several minutes, which makes flywheels the best for this role. Storage with short charging and discharging times, of around a few seconds, can help ensure the appropriate quality of electricity, which is why supercapacitors are the best choice [35,36]. Detailed applications of electricity storage are shown in Table 7.

Table 7. Storing electric energy [35].

Area of Application	Functions of the Storage	Purpose of the Storage/Results Obtained
Electricity grid	co-operation with RES	<ul style="list-style-type: none"> – energy storage in periods of excess production in the source, energy release in the period of the highest demand – compensation for electromagnetic interruptions introduced by the source
	load balancing	<ul style="list-style-type: none"> – reducing maximum loads and the possibility of network congestion – better use of industrial capacity – reduction in power and energy losses – the ability to connect new customers without the need to incur capital expenditure for modernizing and developing the network
Final recipient	voltage regulation and compensation for electromagnetic interruptions	improving the quality of the electricity
	supplying receivers during voltage dips and interruptions to the power supply	reducing the cost of losses resulting from dips and interruptions to the power supply
Prosument	storing energy, in periods of low demand in the system and providing energy to the recipient in periods of maximum demand	reducing the amount of energy consumed from the grid, during periods of maximum demand; reducing energy bills
	load balancing	limiting energy consumption from the power grid
Prosument	voltage regulation and compensation for electromagnetic interruptions	improving the quality of the electricity
	supplying receivers during voltage dips and interruptions to the power supply	reducing the cost of losses resulting from dips and interruptions to the power supply

5. Conclusions

This paper analyses the parameters of photovoltaic installations of different powers, connected to a power system with a rated voltage of 20 kV. The results of simulations in the Matlab/Simulink program are approximately coincident with the theoretical values obtained with formulas. The differences are due to, among other things, inaccurately assumed values of the temperature of the modules during their operation and inaccuracy of

the selected values of parameters of electronic devices in the installation model in the Matlab program. After analysis of the results, it can be concluded that on an average summer's day, the values of the power installation by the reach values, close to the theoretical value under STC conditions. Based on the simulations performed in Matlab/Simulink and the literature sources analyzed in this paper, it can be concluded that single photovoltaic micro-installations have almost no impact on the operation of the power system, and thus on the quality of electricity and power supply reliability. Problems may arise when a large number of micro-installations are connected within a small area of the grid, or when their power rating is significant, which is observed in the daily functioning of the energy system, in the area described in this article. This can lead to interruptions to the system such as voltage fluctuations, voltage asymmetry or higher voltage harmonics distorting the ideal sinusoidal waveform. Voltage dips and voltage interruptions are also observed. All the above-mentioned interruptions may lead to significant deterioration of the quality and the reliability of the power supply and even to the loss of stability of the system operation. Then, it is necessary to consider measures to improve the quality of electricity and compensation of generated reactive power to maintain the parameters of electricity within acceptable limits. Possible corrective actions, with particular emphasis on the use of energy storage facilities, have also been described in this article. Due to the complexity and time taken by the necessary works, further research and simulations for small PV installations (50–500 kW) and numerous PV micro-installations co-operating with the El-en network in a small area are planned by the authors in the future. The results obtained will form the content of the next article.

Author Contributions: Conceptualization, G.T., J.J., A.J. and N.C.-G.; methodology, G.T., J.J., A.J. and N.C.-G.; software, G.T., J.J. and A.J.; validation, W.W., M.W. and N.C.-G.; formal analysis, N.C.-G., W.W., M.W., R.W. and K.S.; investigation, G.T., J.J., A.J. and N.C.-G.; resources, G.T., J.J., A.J. and N.C.-G.; data curation, G.T., J.J. and A.J.; writing—original draft preparation, G.T., J.J., A.J. and N.C.-G.; writing—review and editing, N.C.-G., W.W. and M.W.; visualization, G.T., J.J. and A.J.; supervision, N.C.-G., W.W., M.W., R.W. and K.S.; project administration, W.W., N.C.-G., M.W., R.W. and K.S.; funding acquisition, M.W., R.W., K.S. and N.C.-G. All authors have read and agreed to the published version of the manuscript.

Funding: This research was funded by Warsaw University of Technology.

Data Availability Statement: Data are available in a publicly accessible repository.

Acknowledgments: The authors would like to gratefully acknowledge the reviewers who provided helpful comments and insightful suggestions on a draft of this manuscript.

Conflicts of Interest: The authors declare no conflict of interest. The funders had no role in the design of the study; in the collection, analyses, or interpretation of data; in the writing of the manuscript; or in the decision to publish the results.

References

1. Izdebski, M.; Jacyna, M. An Efficient Hybrid Algorithm for Energy Expenditure Estimation for Electric Vehicles in Urban Service Enterprises. *Energies* **2021**, *14*, 2004. [[CrossRef](#)]
2. Urbaniak, M.; Kardas-Cinal, E.; Jacyna, M. Optimization of Energetic Train Cooperation. *Symmetry* **2019**, *11*, 1175. [[CrossRef](#)]
3. Jacyna, M.; Golebiowski, P.; Urbaniak, M. Multi-option Model of Railway Traffic Organization Including the Energy Recuperation. In *Communications in Computer and Information Science*; Springer: Berlin/Heidelberg, Germany, 2016. [[CrossRef](#)]
4. Łuszczuk, M.; Sulich, A.; Siuta-Tokarska, B.; Zema, T.; Thier, A. The Development of Electromobility in the European Union: Evidence from Poland and Cross-Country Comparisons. *Energies* **2021**, *14*, 8247. [[CrossRef](#)]
5. Jacyna, M.; Zochowska, R.; Sobota, A.; Wasiak, M. Scenario Analyses of Exhaust Emissions Reduction through the Introduction of Electric Vehicles into the City. *Energies* **2021**, *14*, 2030. [[CrossRef](#)]
6. Sweeting, W.J.; Hutchinson, A.R.; Savage, S.D. Factors affecting electric vehicle energy consumption. *Int. J. Sustain. Eng.* **2011**, *4*, 192–201. [[CrossRef](#)]
7. Wasiak, M.; Zdanowicz, P.; Nivette, M. Research on the effectiveness of alternative propulsion sources in high-tonnage cargo transport. *Arch. Transp.* **2021**, *60*, 259–273. [[CrossRef](#)]
8. Karoń, G. Safe and Effective Smart Urban Transportation-Energy Flow in Electric (EV) and Hybrid Electric Vehicles (HEV). *Energies* **2022**, *15*, 6548. [[CrossRef](#)]

9. Karoń, G. Energy Smart Urban Transportation with Systemic Use of Electric Vehicles. *Energies* **2022**, *15*, 5751. [[CrossRef](#)]
10. Barchański, A.; Żochowska, R.; Kłos, M. A Method for the Identification of Critical Interstop Sections in Terms of Introducing Electric Buses in Public Transport. *Energies* **2022**, *15*, 7543. [[CrossRef](#)]
11. *World Cities Report 2022: Envisaging the Future of Cities, United Nations Human Settlements Programme (UN-Habitat)*; United Nations: New York, NY, USA, 2022.
12. Kissa, G.; Jansenb, H.; Castaldoc, V.L.; Orsia, L. The 2050 City. International Conference on Sustainable Design, Engineering and Construction. *Procedia Eng.* **2015**, *118*, 326–355. [[CrossRef](#)]
13. Xiang, C.; Matusiak, B.S. Façade Integrated Photovoltaics design for high-rise buildings with balconies, balancing daylight, aesthetic and energy productivity performance. *J. Build. Eng.* **2022**, *57*, 104950. [[CrossRef](#)]
14. Anzalchi, A.; Sarwat, A. Overview of technical specifications for grid-connected photovoltaic systems. *Energy Convers. Manag.* **2017**, *152*, 312–327. [[CrossRef](#)]
15. Macêdo, W.N.; Zilles, R. Influence of the power contribution of a grid-connected photovoltaic system and its operational particularities. *Energy Sustain. Dev.* **2009**, *13*, 202–211. [[CrossRef](#)]
16. Kabiri, R.; Holmes, D.G.; McGrath, B.P. The influence of pv inverter reactive power injection on grid voltage regulation. In Proceedings of the 2014 IEEE 5th International Symposium on Power Electronics for Distributed Generation Systems (PEDG), Galway, Ireland, 24–27 June 2014; pp. 1–8. [[CrossRef](#)]
17. Liu, W.; Peng, D.; Bu, G.Q.; Su, J. A survey on system problems in smart distribution network with grid-connected photovoltaic generation. *Power Syst. Technol.* **2009**, *19*, 1–5.
18. Buzdugan, M. Voltage Dips in Power Quality—A Brief Review. In Proceedings of the 2019 AEIT International Annual Conference (AEIT), Florence, Italy, 18–20 September 2019; pp. 1–6. [[CrossRef](#)]
19. Good, C.; Kristjansdóttir, T.; Wiberg, A.H.; Georges, L.; Hestnes, A.G. Influence of PV technology and system design on the emission balance of a net zero emission building concept. *Sol. Energy* **2016**, *130*, 89–100. [[CrossRef](#)]
20. Gunduz, H.; Jayaweera, D. Reliability assessment of a power system with cyber-physical interactive operation of photovoltaic systems. *Int. J. Electr. Power Energy Syst.* **2018**, *101*, 371–384. [[CrossRef](#)]
21. Zeb, K.; Uddin, W.; Khan, M.A.; Ali, Z.; Ali, M.U.; Christofides, N.; Kim, H.J. A comprehensive review on inverter topologies and control strategies for grid connected photovoltaic system. *Renew. Sustain. Energy Rev.* **2018**, *94*, 1120–1141. [[CrossRef](#)]
22. Mróz, M. Wahania napięcia jako kryterium przyłączania elektrowni do sieci dystrybucyjnych. AGH 2018. Available online: <http://www.sep.krakow.pl/biuletyn/nbiuletyn/nr61ar2> (accessed on 15 October 2022).
23. Jagusiak, M.; Drózdź, T.; Nawara, P.; Kielbasa, P.; Lis, S.; Wrona, P.; Necka, K.; Oziembłowski, M. Kompatybilność elektromagnetyczna w pomiarach energii elektrycznej. *Przegląd Elektrotechniczny* **2016**, *1*, 139–144. [[CrossRef](#)]
24. Pruski, P.; Paszek, S. Analysis of Waveforms in a Power System at Asymmetrical and Symmetrical Short-Circuits in a Transmission Line. *Acta Energetica* 2019, *1/38*, 17–22. [[CrossRef](#)]
25. Büdenbender, K.; Braun, M.; Schmiegel, A.; Magnor, D.; Marcel, J.C. Improving PV-integration into the distribution grid-contribution of multifunctional PV-battery systems to stabilised system operation. In Proceedings of the 25th European Photovoltaic Solar Energy Conference and Exhibition, Valencia, Spain, 6–10 September 2010; pp. 4839–4845.
26. de Silva, G.D.O.; Hendrick, P. Photovoltaic self-sufficiency of Belgian households using lithium-ion batteries, and its impact on the grid. *Appl. Energy* **2017**, *195*, 786–799. [[CrossRef](#)]
27. de Lima, L.C.; de Araújo Ferreira, L.; de Lima Moraes, F.H.B. Performance analysis of a grid connected photovoltaic system in northeastern Brazil. *Energy Sustain. Dev.* **2017**, *37*, 79–85. [[CrossRef](#)]
28. Bouacha, S.; Malek, A.; Benkraouda, O.; Arab, A.H.; Razagui, A.; Boulahchiche, S.; Semaoui, S. Performance analysis of the first photovoltaic grid-connected system in Algeria. *Energy Sustain. Dev.* **2020**, *57*, 1–11. [[CrossRef](#)]
29. Sharma, R.; Goel, S. Performance analysis of a 11. 2 kWp roof top grid-connected PV system in Eastern India. *Energy Rep.* **2017**, *3*, 76–84. [[CrossRef](#)]
30. Detailed Model of a 100-kW Grid-Connected PV Array. Available online: <https://www.mathworks.com/help/phymod/sps/ug/detailed-model-of-a-100-kw-grid-connected-pv-array.html> (accessed on 26 January 2022).
31. Moacyr, A.G.; de Brito, L.P.; Sampaio, L.G., Jr.; e Melo, G.A.; Canesin, C.A. Comparative Analysis of MPPT Techniques for PV Applications. In Proceedings of the 2011 International Conference on Clean Electrical Power (ICCEP), Ischia, Italy, 14–16 June 2011. [[CrossRef](#)]
32. Kjaer, S.B.; Pedersen, J.K.; Blaabjerg, F. Power inverter topologies for photovoltaic modules—a review. In Proceedings of the 2002 IEEE Industry Applications Conference. 37th IAS Annual Meeting (Cat. No. 02CH37344), Pittsburgh, PA, USA, 13–18 October 2002; Volume 2, pp. 782–788. [[CrossRef](#)]
33. Mehiri, A.; Bettayeb, M.; Hamid, A.K.; Ardjal, A. Fractional nonlinear synergetic control for DC-link voltage regulator of three phase inverter grid-tied PV system. In Proceedings of the 5th International Conference on Renewable Energy: Generation and Applications (ICREGA), Al Ain, United Arab Emirates, 25–28 February 2018.
34. SPR-305E-WHT-D Solar Panel from SunPower. Available online: https://www.possharp.com/spr-305e-wht-d-solar-panel-from-sunpower_p1621616600d.aspx,11.2022 (accessed on 10 November 2022).

35. Kowalak, R.; Malkowski, R.; Czapp, S.; Klucznik, J.; Lubosny, Z.; Dobrzynski, K. Computer-aided analysis of resonance risk in power system with Static Var Compensators. *Prz. Elektrotechniczny* **2016**, *1*, 22–27. [[CrossRef](#)] [[PubMed](#)]
36. Kubek, P.; Rzepka, P.; Szablicki, M.; Wasilewski, J. Electric Energy Storages—An Innovative Idea for Frequency Stabilization in Power System. *Autom. Electrotech. Disturb.* **2016**, *7*, 6–11. [[CrossRef](#)]

Disclaimer/Publisher’s Note: The statements, opinions and data contained in all publications are solely those of the individual author(s) and contributor(s) and not of MDPI and/or the editor(s). MDPI and/or the editor(s) disclaim responsibility for any injury to people or property resulting from any ideas, methods, instructions or products referred to in the content.